CHAPTER 4

Optimization of Facet-Coating for Laser Diode

4. Optimization of Facet-Coating for Laser Diode

One of the most crucial aspects of high-power laser diode technology is that of protecting laser facets from degradation to ensure long-term reliable operation. This is achieved by dielectric thin film coating on the facets. Facet-coating also helps extracting the maximum laser output from only one facet to make it efficiently usable. This chapter discusses the degradation mechanism at laser diode facets and optimization of facet-coating conditions. Investigations of anti-reflection (AR) and high-reflection (HR) coatings have been carried out on front and back facets of laser diodes, respectively, and the effects of facet-coatings on laser diodes' characteristics have been studied. An in-situ reflectivity measurement setup has been established and is described in details.

4.1 Degradation of Laser Diodes

During the operation of high-power laser diode, the output power under a constant driving current drops off indicating the device-degradation. There are several types of degradation modes depending on the initial period of degradation, degradation rate, and the degree of degradation. Figure 4.1 illustrates three different degradation modes [1]: gradual, rapid and catastrophic degradation.

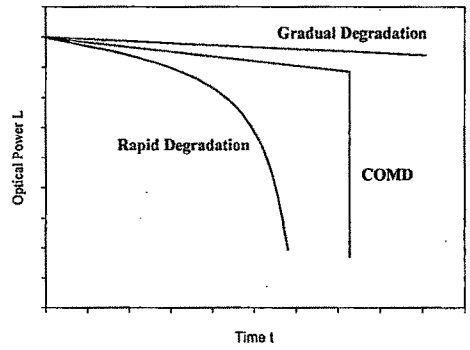

Figure 4.1: Various degradation modes of laser diode.

The rapid degradation can be detected by a very fast decrease in output power at a constant driving current. The ultimate lifetime of the laser diode is determined by gradual

degradation which occurs over a long period. The maximum optical power of high-power laser diodes, however, is mostly limited by the catastrophic optical mirror damage (COMD). The understanding of COMD mechanism is crucial, since it is one of the major killing factors for high-power laser diodes.

4.1.1 COMD Mechanisms

The occurrence of COMD is attributed to thermal runaway process that takes place at the facet [2]. The mechanism of COMD can be explained with the help of various feedback loops at the cleaved laser diode facets as shown in figure 4.2.

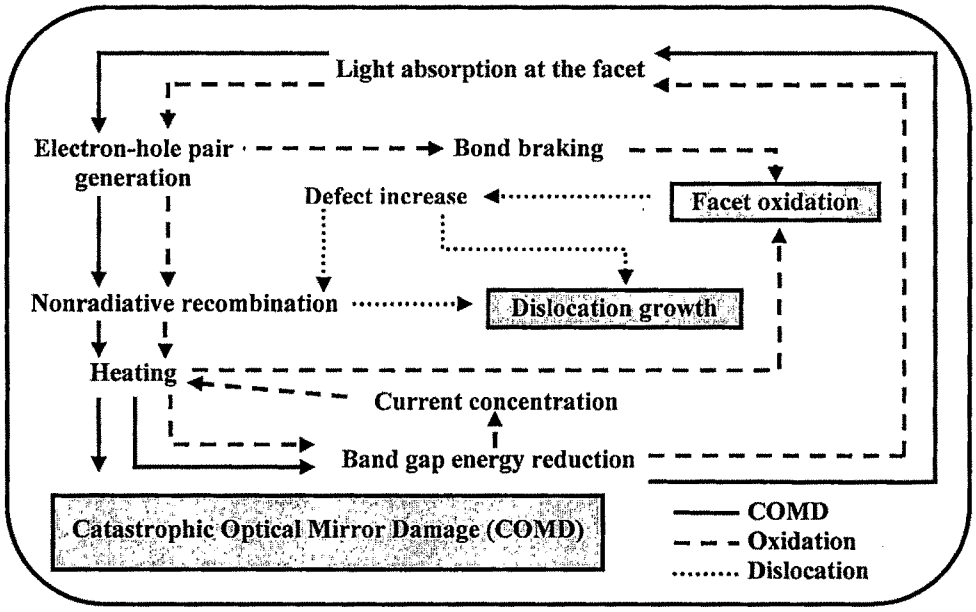

Figure 4.2: COMD mechanism in edge-emitting laser diode.

Processes in these loops progressively damage the facets of laser diode and ultimately lead to the device failure. The initial absorption at the facets is started by deep centers (interface states) at the semiconductor–insulator interface. These centers can increase in concentration by photo-assisted oxidation of the semiconductor material. The mirror facet also contains a large amount of nonradiative recombination centers due to oxides and segregated atoms at the surface [3,4]. The electron–hole pairs, generated by the absorption of stimulated emission, recombine nonradiatively at these centers in the facet region. This nonradiative surface recombination results in the facet-heating and

consequently the bandgap shrinkage. This band-gap reduction increases the light absorption at the facets, and a self-killing positive-feedback loop develops. This effect is also enhanced by current crowding at the facet due to the lower band gap [5]. Moreover, the heating at the facet region is concentrated in a very small volume and hence it can lead to the thermal damage of the facet very quickly, the so-called COMD.

COMD is quite a complex phenomenon and depends on many parameters. The temperature of the mirror facet increases with the injection current and high output optical flux. Experimental investigations about the local temperature are usually carried out by micro-Raman spectroscopy [5], reflectance modulation [6] and micro-photoluminescence (μ-PL) [7] at the facet. The theoretical calculations about the temperature enhancement at the facets [8,9] are referred in support of the experimental investigations. These investigations reveal that the thermal runaway initiates at some critical temperature depending upon the semiconductor material system. The facet temperatures were found to depend on the surface recombination velocity showing the importance of the facet treatment for COMD [8]. It is also clear that the temperature rise is restricted to the facet region and beyond a certain distance from the facet inside the cavity, typically 1 μm, a significant cooling is observed, which means that the cavity is cold as compared to the facets [8].

Laser diodes also exhibit compositional changes at the facet during its life. One of the main concerns for COMD is the fast oxidation of the mirror facets. Oxidation is enhanced by the temperature. Further, the oxidation rate at the facets is proportional to the light output density. The oxidation of the facet creates point defects in the active layer near the facet, which, on saturation, generate dark line defects (DLDs) assisted by recombination enhanced defect reactions (REDR). COMD is generally associated with the generation of these DLDs close to the facet.

The oxidation of the facets also depends upon the nature of the semiconductors forming the active regions and the cladding layers. Al-free laser structures such as InGaAs, GaAs, and InGaP based lasers are expected to have improved reliability and stability due to a lower generation rate of dark line defects and reduced surface oxidation during processing and operation [10,11]. COMD is still considered to be the prominent failure mechanism even in Al-free lasers. One can define the P_{COMD} level as the

maximum output power density allowed without COMD. The COMD level is increased with indium content of the active region and decreases with Al content [12]. COMD is also related to the type of laser structure. In particular, both, the thickness of the active region and the cavity length, have influence on the COMD level. Quantum-well (QW) laser facets are more oxidized than the facets of double-heterojunction lasers [13].

4.2 Facet Passivation for Laser Diode

Various approaches are being pursued to reduce the probability and rate of facet degradation. One way to protect the laser diode facet from possible COMD is to decrease the initial light absorption at the facet by increasing the band gap near the facet. For example, the band gap value in the facet region can be increased by strain relaxation near the facets of tensile-strained QW [14]. However, the effect is not very prominent and tensile-strained QWs cannot always be implemented. Diffusion- or implantation-enhanced interdiffusion between the QW and the surrounding material is another possibility to achieve a larger band gap in the facet region [15]. However, the interdiffusion is a high temperature process and requires more than 800 °C temperature. Thus, it is very difficult to integrate the process step into laser diode manufacturing. A third technology is the re-growth of a window section at the facet with a semiconductor material having a higher band gap. This is further involved method and connected with the single laser diode bars instead of a full wafer processing [16], thus increasing the manufacturing cost and complexity.

Another way to increase the P_{COMD} level is by reducing surface-recombination velocity. This involves a rather complicated technology and usually is not in line with an industrial low-cost production of laser diodes. One possibility of reducing surface recombination velocity is cleaving of wafers in ultrahigh vacuum followed by deposition of an appropriate passivation layer on the surface [17]. Alternatively, the surface can be treated with sulfuric reagents to replace the nonstable oxide by a more stable compound [18]. However, these processes are not very popular either because of their complexities or due to possibility of damage during the surface treatment.

The simplest way to protect the laser diode facet and to improve the reliability of the laser diode is to coat the facets with dielectric layers. The lifetime of the device is significantly improved on coating the mirror facets. This coating suppresses the facet oxidation and subsequently reduces the surface recombination velocity.

Moreover, in the case of laser diodes, the resonator cavity is formed by the cleaved facets of the semiconductor crystal. The reflectivity of both the pure cleaved facets is nearly 32%. Hence, the laser diodes emit light equally from both the facets. However, in most of the practical applications, it is generally not possible to use the light from both facets of the laser. In order that, the light is emitted from only one of the facets, one facet of the laser is coated with anti-reflection (AR) coating and the other with high-reflection (HR) coating. Figure 4.3 schematically illustrates the facet-coatings for a laser diode. The AR coating on the front facet of the laser diode increases the light output from this facet. On the other hand, the HR coating on the rear facet reflects the laser light back into the cavity and reduces the output power from that facet.

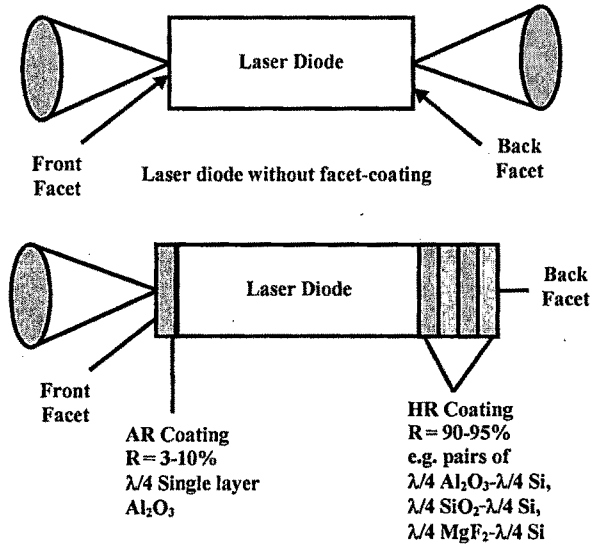

Figure 4.3: Schematic illustration of facet-coating on laser diode chip.

The facet-coating process has to fulfill some crucial requirements. First, the desired reflectivities, typically greater than 90% at the rear facet and values from 3% to 10% at the front facet, should be realized. Moreover, the process must be reproducible and technologically suitable for mass-production. The coatings also have to exhibit a

number of properties, e.g. chemical and mechanical stability, good adhesion to the facet surface, low mechanical stress, high transparency at the emission wavelength, and an excellent behavior with respect to lifetime and COMD. For optical communication systems it is also necessary that the beam characteristics of the laser devices do not change by facet-coating.

The facet-coating with dielectric thin films protects the facets of laser diodes from environmental influences. It reduces the chemical and thermal effects at the laser facets and increases the lifetime of the devices. However, even for lasers with facet-coating, nonradiative recombination occurs via the electronic states at the interface between the laser material and the coating. Consequently, COMD also occurs in lasers with facet-coating films, although the COMD power level increases because of the lower density of the interfacial states compared to the density of the surface states and because of thermal conductivity of the films [19,20]. So a suitable design with respect to good thermal conductivity at the facet and good adhesion to the facet together with chemical and mechanical stability can shift the P_{COMD} level to high output power and increases the lifetime of the device.

In fact, the facet-coating allows reliable lasers in nonhermetic packages which could not only eliminate the costs associated with hermetic packaging but also open new low-cost alternatives in optoelectronic packaging. Basically, non-degradable facet-coatings capable of protecting the laser from ambient and maintaining the facet-coating reflectivity are required to avoid premature device failure. Ideally, the facet-coatings, especially for nonhermetically packaged lasers, should be self-passivated, dense and with good mechanical properties to resist exposure to heat and humidity [21].

Facet-coating reduces the degradation rate significantly [22,23]. The lasing transition of QW laser can also be tailored to take place either between the $n = 1$ or $n = 2$ sub-band by proper design of the facet reflectivity [24] The laser modulation bandwidth can also be increased by reflectivity modulation of the facets [25]. This can be achieved by means of increasing the relaxation oscillation frequency of the laser with the help of optimum facet reflectivity modulation. Coated samples further show a narrower width of the mode spectra peak and better side mode suppression. Beam divergence of the axis

perpendicular to the active region was reduced by 30% when an AR coating of silicon oxide was applied [26].

4.3 Optical Thin Films for Laser Diode Facets

The reflectivity modulation by facet-coating employs the principle of interference in dielectric thin films. Optical interference in a thin film can be explained in terms of wave theory of light. When a light wave traveling in a certain medium, say air with refractive index n_0, encounters a medium, with different refractive index n_1, a portion of incident wave is reflected at the interface. The amplitude of the reflected wave, which is equivalent to the electric field strength, is computed from an equation developed in 1816 by the French physicist Augustin Jean Fresnel. The amplitude of this reflected portion depends on the refractive indices of both media and can be given for normal incidence as,

$$\rho = \frac{n_0 - n_1}{n_0 + n_1} \tag{4.1}$$

The Fresnel reflection coefficient ρ in the above equation is real; its sign, which depends on the difference between n_0 and n_1, determines whether there is a phase shift between the corresponding wave and the incident wave. One can modify the reflectance of a surface by coating the surface with single or multilayer dielectric thin films. In a multilayer coating, a portion of the incident wave is reflected at each of the interfaces. The phase difference between the incident and reflected light, depending upon the film's thickness and film's refractive index, also called optical thickness, causes either constructive or destructive interference and subsequently the reflectance of the coated surface decreases or increases respectively.

4.3.1 Anti-Reflection Coating

Anti-reflection coating is indispensable for realizing laser diodes with high-power, super luminescent diodes (SLDs) and semiconductor laser amplifier. Laser diodes with one or both of their facet reflectivity reduced by AR coating are transformed from oscillating cavities into gain media. Devices with AR coating on one facet are commonly used in external cavity lasers for narrow line width sources [27] and for mode locking [28]. Traveling wave optical amplifiers [29,30] with AR coatings on both facets require very

low reflectivity to ensure reasonably high gain while maintaining small wavelength dependent ripple in gain [31]. High-quality AR coatings reduce residual regenerative amplification, eliminate parasitic oscillations, and delay the onset of filamentation in broad-area devices [32]. The AM noise, which is a serious problem in operation of index-guided AlGaAs lasers, is found to be strikingly reduced by the AR coating on the facets. This effect is shown to result from the longitudinal multimode operation due to the reduced facet reflectivity [33]. Laser devices with an AR coating on one facet can be used for spectroscopy when combined with a grating as external reflector, since they are continuously tunable over a wavelength range of more than 25 nm [34].

The AR coating on the front facet of the laser diode ensures that very little light is lost from the output beam at the front facet. It works on the principle of destructive interference between the light reflected from the upper and the lower surface of the thin film of dielectric material deposited on the front facet. The coating is designed so that the relative phase shift between the beam reflected at the upper and lower boundary of the thin film is 180°. Destructive interference between the two reflected beams occurs, canceling both beams before they exit the surface as shown in figure 4.4. Thus, it reduces the reflection and increases the transmission at substrate-air interface.

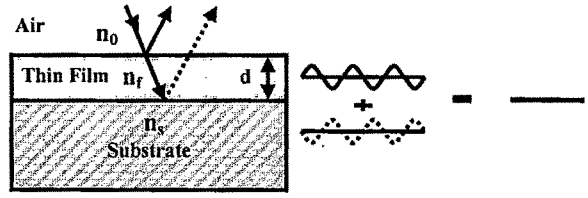

Figure 4.4: Destructive interference in AR coating.

The reflection properties of a coating depend upon the wavelength of light being used, λ, thickness of the film, d, angle of the incident light, θ, refractive index of the substrate, n_s, and that of the film, n_f. The condition of destructive interference demands that the optical thickness of the AR coating film is one quarter of lasing wavelength ($\lambda/4$) of the laser diode in order to achieve the desired path difference of one half wavelength between the reflected beams, which leads to their cancellation. So, the physical thickness of the film is,

$$d = \frac{\lambda}{4n_f} \tag{4.2}$$

For normal incidence of light, this design for AR coating is called quarter-wave optical thickness (QWOT). For minimum reflectance, the refractive index of the film n_f should be chosen so that,

$$n_f = (n_0 n_s)^{\frac{1}{2}} \tag{4.3}$$

The normal reflectance reflectivity, R, of a single layer AR film is given by the formula [35].

$$R = \frac{(1-n_s)^2 \cos^2(\delta) + \left(\frac{n_s}{n_f} - n_f\right)^2 \sin^2(\delta)}{(1+n_s)^2 \cos^2(\delta) + \left(\frac{n_s}{n_f} + n_f\right)^2 \sin^2(\delta)} \tag{4.4}$$

where,

$$\delta = 2\pi \frac{n_f d}{\lambda} \tag{4.5}$$

By changing the film material, the minimum of the reflectivity can be adjusted in a wide range. The reflectivity can be further reduced by multilayer AR coating. However, for edge-emitting laser diode application, the reflectivity achieved by single layer AR coating is sufficient. Further, the single layer AR coating design is very simple and cost effective. Hence, we used single layer AR coating for reflectivity modulation and passivation purpose on our laser diodes.

4.3.2 High-Reflection Coating

The high-reflection coating is used to stop the light emission from the rear facet of laser diode and to reflect most of the light back into the cavity. To increase the reflectivity of a laser facet it is necessary to use more than one dielectric coating layer. So an HR coating is composed of a number of bi-layers with different refractive indices. The HR coating depends on complete addition of light reflected at the upper and lower surfaces of the thin film. The reflections at successive boundaries of multi-layers reappear at the front surface all in phase so that they recombine constructively. This implies that the effective reflectance of the assembly can be made very high and it increases by increasing the number of bi-layers.

The multilayer stack for HR coating is a stack of alternating films of high (n_H) and low (n_L) refractive index bi-layers with each high and low index layer of QWOT at the selected wavelength. The reflectance at the wave length λ is given by [36],

$$R_{2S} = \left[\frac{n_s^F - n_0}{n_s^F + n_0}\right]^2 \tag{4.6}$$

where, $F = \left(\frac{n_H}{n_L}\right)^{2s}$ and s is the number of bi-layer pairs. The actual structure of multi-layer stack is GaAs substrate-LHLH...LH-Air. To create the highest reflectance in the fewest number of layers, it is desirable that the ratio (n_0/n_1) be as large as possible. The reflectivity increases with the number of bi-layer pairs. To reduce mechanical stress and to increase the stability of the coating, it is necessary to choose a layer material for good adhesion and reduce the number of layers to the lowest possible number which is necessary to reach the desired reflectivity.

4.3.3 Materials for AR-HR Coatings

From a technological point of view, the coating material should be depositable on the facets without causing any damage to the underlying semiconductor material and without removing the passivation material and hence passivation effects. On the other hand the adhesion has to be very good. To minimize the reflectivity with a single layer, the coating material should have a refractive index close to the geometric mean between the effective index of the waveguide and the index of air, as given in equation (4.3).

The initial choice of the coating materials is based largely on the index of refraction and transmission range of the material. Low absorption is obviously needed so that material does not absorb light at the wavelength of interest. This is the reason why dielectric stack of low and high refractive index materials is preferred over metals for HR coating even though metals provide higher reflectance easily. The transmission range is limited at short wavelengths by the band gap of the material and at long wavelength by molecular vibrational absorption. Thus, the band gap of the material should be much higher than the laser photon energy. Below the band edge, the level of absorption is determined by defect levels and requires optimization of coating conditions. Moreover,

the coating material should exhibit long-time stability to prevent the diffusion of components from the environmental atmosphere into the active layer under high-power operation.

Many materials have been reported for the AR coatings on the laser facets. For example, Silicon nitride [37], and Ga_2O_3 [38] were used to obtain AR coating by means of a single layer. We have used alumina (Al_2O_3) as a low refractive index material in most of our experiments. The refractive index of Al_2O_3 is about 1.66 which is close to the required refractive index for single layer AR coating on laser diode facet. The aluminum oxide has a relatively high dielectric constant (k=~10), wide band gap of about 10 eV, and high chemical stability [39]. Its useful transmissive range extends from 50nm to 6 μm. It also exhibits low permeability to alkali ions, very high resistivity, high resistance to radiation, and has high thermal conductivity and stability with a thermal expansion coefficient of 8.4×10^{-6}/°C (20-500°C) and a density of 3.97 gm/cm^3. Also the hardness and the high corrosion resistance favor Al_2O_3 as passivation layer.

Coating performance is strongly tied to the ratio of the refractive indices of the materials making up the stack in case of multilayer HR coating. High ratios provide wider bandwidth and require fewer layers to obtain specific reflectance. Thus, for HR coating, the other material should have high refractive index. We have used silicon as a high refractive index material. The refractive index of Silicon is about 3.4, giving more than 90% reflectivity with only three pairs of Al_2O_3-Si.

The deposition of AR and HR coatings on the facets of laser diode involve thin film deposition technology. We have carried out the facet-coating on laser diodes using e-beam evaporation technique. The next section discusses issues related to optical thin film deposition using e-beam and optimization of coating conditions for laser diode facets.

4.4 Thin film Deposition Technique

Any thin film deposition process involves three main steps: (i) production of the appropriate atomic, molecular or ionic species, (ii) their transport to the substrate through a medium, and (iii) condensation on the substrate.

The growth process may be summarized as consisting of a statistical process of nucleation, i.e., surface-diffusion controlled growth of the three dimensional nuclei, and formation of a network structure and its subsequent filling to give a continuous film. The initial nucleation and growth stages are determined by the thermodynamic parameters of the deposit and the substrate surface. Thin films can be realized by various deposition techniques like physical vapor deposition (PVD), chemical vapor deposition (CVD), sol-gel technique, etc.

4.4.1 Physical Vapor Deposition

The term Physical Vapor Deposition (PVD) denotes vacuum deposition process where the coating material is evaporated by some technique and the vapor phase is transported to the substrate by physical means, forming a thin film coating. PVD of thin films relies on the removal of atoms from a solid or a liquid by energetic means, and the subsequent deposition of those atoms on a nearby surface. The deposition is carried out essentially in a vacuum of such magnitude that the mean free path of the ambient gas molecules is greater than the dimension of the deposition chamber and the source to substrate distance. PVD processes generically involve individual atoms or perhaps small clusters of atoms which are not normally found in the gas phase. Typically these atoms are removed from a solid or liquid source, transit an evacuated chamber, and impinge on a solid surface at which point the atoms stick and form a film. The means to remove the atoms from the original source can be by thermal heating of the source or energetic particle bombardment by electrons, atoms, ions, molecules, or photons. The removal process can be thermodynamic, as is the case typically with evaporation and ablation, or may be the result of a sequence of energetic collisions near the surface which results in the kinetic ejection of atoms from the source; a process generically called sputtering. PVD is a line-of-sight process in which atoms travel from a metallic source to the substrate on a straight path. Once the atoms or small atom clusters are removed from the original surface, they travel within an evacuated chamber until they impinge on a solid surface, at which point there is a probability for condensation. Depending on the method of applying heat to the source material, the PVD can be classified in various techniques such as thermal evaporation, electron-beam (e-beam) evaporation, sputtering, pulsed laser deposition, etc.

4.4.1.1 Electron Beam Evaporation Technique

AR coatings on laser diodes have previously been demonstrated using RF sputtered silicon nitride [37] and lead silicate [40]. RF sputtering is a convenient PVD method since deposition rate is slow, enabling easy control over the thickness, and since the films are uniform and show good adhesion properties. However, RF sputtering suffers from the fact that multilayer coatings, which is essential for HR coatings, can not be carried out easily with this technique or it requires very complex system. Moreover, it is difficult to incorporate in-situ monitoring in the system since the plasma is complex and easily disturbed. In addition, dielectric target for RF sputtering systems tend to be non uniform, making it difficult to maintain reproducibility in the film index. Deposition by e-beam evaporation is an alternative method which can solve some of these problems. A large variety of dielectric materials can be deposited by e-beam evaporation and it allows multilayer deposition. The incorporation of in-situ monitoring system is easy in e-beam system.

In this system, the material to be evaporated is placed into a graphite or appropriate crucible in an open metal cup, called hearth, which is water-cooled. The energetic e-beam, emitted by e-gun through thermionic emission from a tungsten filament, is accelerated, directed, and focused, onto the source material by means of permanent or electro-magnet. The energetic e-beam imparts energy to the source material, melts it and evaporates it. Evaporative deposition occurs simply by placing a sample in the direct line-of-sight of the source. Typically, there is a modest distance of about 10 to 50 cm between the source and sample for the practical reasons of allowing a larger deposition area and to limit sample heating by optical radiation from the source. The flux is emitted from the source with roughly a cosine distribution. Most evaporative deposition systems require high vacuum to operate efficiently. Aside from the issue of impurity incorporation, it is desired that the mean free path of the evaporant-flux exceeds the distance from the source to the sample. This reduces in-flight scattering with the background gas, which can lead to reduced deposition rates. The scattering, which defines the mean free path, is related to the density and pressure of atoms and molecules in the gas phase. From the kinetic theory of gas, the mean free path, mfp, is calculated as [41]:

$$mfp = \frac{k_B T}{\sqrt{2}\,\mathrm{Pr}^2 \pi} \tag{4.7}$$

where k_B is Boltzmann constant, T is absolute temperature, r is molecular diameter, and P is pressure in Pascal. The scattering probability is given as fraction N/N_0 of molecules that are scattered in distance "d" during their travel through gas.

$$\frac{N}{N_0} = 1 - e^{\frac{-d}{mfp}} \tag{4.8}$$

where, N_0 is total number of molecules, N is number of molecules that suffers collisions, d is distance between source and substrate.

- **Advantages of e-beam evaporation technique**

1. The temperature at the focused spot can be raised to as high as 3000°C. At such a high temperature most of the refractory metals, oxides and compounds having high melting point can be evaporated.
2. Since the temperature is high only at a focused spot, rest of the material including the crucible remain cool and thus there is reduced contamination.
3. Multi-hearth evaporation is possible and thus very useful in multilayer coatings.
4. Offers many desirable characteristics such as high evaporation rate, relatively highly dense coating, good composition control, columnar and polycrystalline microstructure, good surface finish and a uniform microstructure.

- **Disadvantages of e-beam evaporation technique**

1. The electron energy is sufficient to ionize residual gas or evaporant molecules encountered along the way. Since ionization causes loss of beam-energy and beam-focus, the pressure in the vacuum chamber must be below 10^{-4} torr, preferably 10^{-6} torr.
2. Generation of X-rays by the e-beam.

4.5 Optimization of Coating Conditions for Laser Diode

Optical coatings on laser diode facets require careful design and high degree of control over the deposited thin film parameters. Low absorption coating requires compositionally pure starting materials and clean vacuum chamber. The e-beam evaporation offers very

good purity and avoids the contamination from crucible and other nearby materials to the source by making a self-forming *crucible* out of the evaporant material itself. The incident e-beam has sufficient energy to melt a relatively small spot on the top of the material kept in the crucible in a water-cooled hearth. A small area of the liquid is heated well above the melting point at the surface, but the temperature at the bottom of the liquid is much colder, such that the adjacent material does not even reach the melting point. Therefore, the molten metal is only in contact with a de-facto crucible made of the same material, and hence any chemical reactions with contaminants are eliminated.

The film structure plays a big role in deciding the optical performance of the film. Columnar structure of the film results in many properties detrimental to thin film performance including channels for moisture incorporation, cracks which can influence local electric field distribution, surfaces which are chemically active, and boundaries which may be mechanically unstable. The substrate is rotated with a constant rpm during evaporation using a stepper motor inside the vacuum chamber to avoid columnar growth.

Optical coating for laser diode should be morphologically isotropic to provide homogeneous material properties. The major process parameters affecting morphology are substrate temperature and evaporation rate. Substrate temperature affects the absorption, diffusion, composition, nucleation, and growth of the thin film. We optimized the substrate temperature for the deposition of dielectric thin films on the laser diode facets.

The deposition rate affects the coating morphology and stoichiometry of the film. The electron gun is known for causing 'spatter' from the source during evaporation. Spattering occurs because the electron beam loses more than half of its energy in the last quarter of its penetration depth. At high e-beam power, the temperature is higher underneath the free surface, generating pressure differentials that are revealed via explosions. Under certain conditions, molten particles can be seen ejected from the source. The spattering is minimized by reducing the e-beam surface intensity and thereby reducing the evaporation rate. Thus facet-coating is carried out at low evaporation rate.

The intensity may also be decreased by increasing the surface area of the beam impact footprint or by decreasing the beam energy. A broad e-beam footprint is also

advantageous because the source materials evaporates and depletes more uniformly. The former reduces the coating thickness irregularities over the surface area of the substrate. The latter helps to maintain thickness control over a large number of coating layers. To further improve these conditions, we used sweeping e-beam at high frequency on the material surface instead of steady electron beam.

4.6 Experimental

The AR and HR coatings were deposited in an electron beam evaporation system using 6 KW electron beam evaporator in a high vacuum coating unit (Hind High Vacuum Co. (P) Ltd.). The coating unit is equipped with 270^0 bend e-beam gun facility. Figure 4.5 shows the actual picture of the vacuum coating unit.

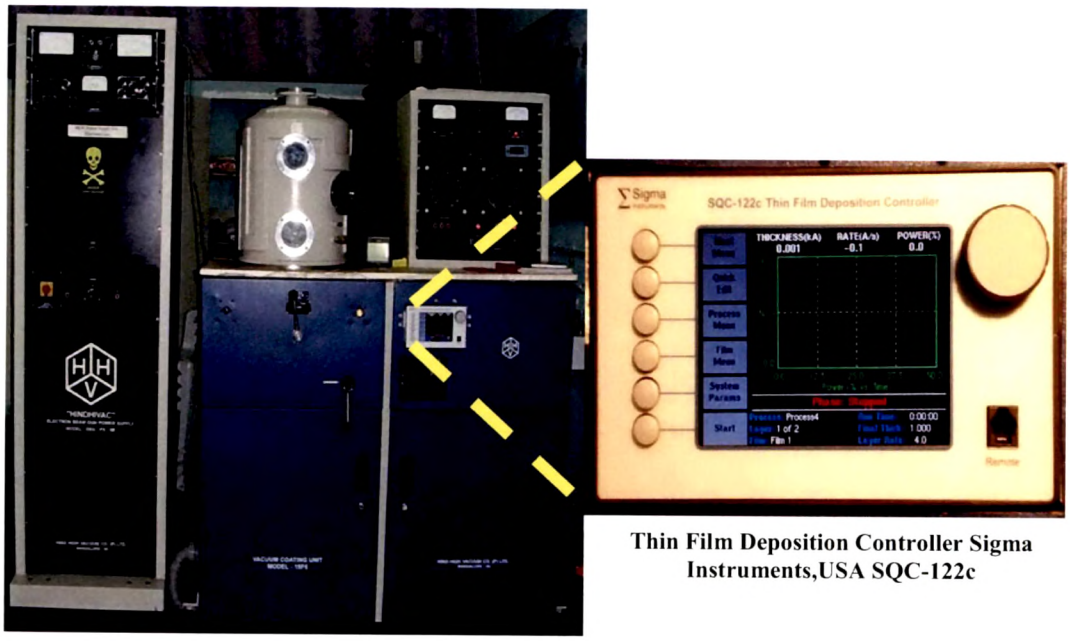

Thin Film Deposition Controller Sigma Instruments,USA SQC-122c

Figure 4.5: High vacuum coating unit with 270^0 bend e-beam gun facility.

As shown in the picture, the electron beam evaporation system is interfaced with SQC-122c SIGMA Thin Film Deposition Controller to precisely monitor and control the thickness and deposition rate of the thin film. The thickness measurement involves piezoelectric quartz crystal placed inside the vacuum chamber. The oscillating frequency of the quartz crystal declines from its original frequency, i.e. 6 MHz, as coating materials

are deposited on the crystal. The rate of change of the crystal frequency depends on the mass of the deposited material. Consequently, the thickness of the coating on the crystal can be calculated by measuring the fall of the crystal's oscillation frequency, area of the crystal exposed to the film and the density data of the material. The crystal is positioned at the center of the coating chamber and the coating thickness on the crystal is used to calculate the coating thickness on the sample. The coating plant is pumped down to achieve a pressure up to $3x10^{-6}$ mbar using an oil diffusion pump backed by a rotary pump. A special jig has been fabricated to coat the end facets of the laser bars. The jig uses two silicon wafers to hold the laser diode bar with spring action of two springs. Figure 4.6 shows the pictures of jig to hold laser diode bar for facet-coating.

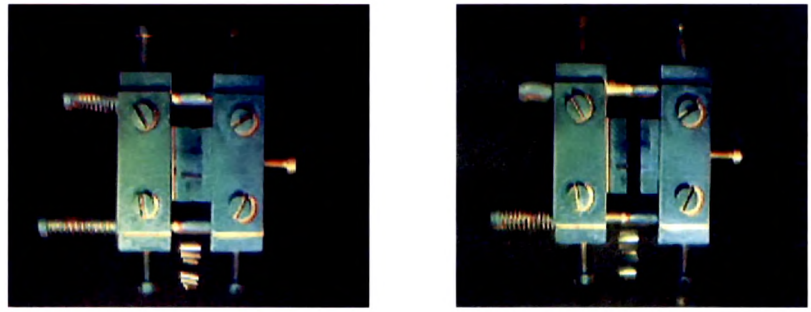

Figure 4.6: Jig to hold laser diode during facet-coating.

The substrates and laser diode are rotated with 120 rpm inside the vacuum chamber during deposition with the help of a stepper motor in order to get uniform coating. AR-HR films have been deposited at 200 °C substrate temperature with the constant rate of 4 Å/sec unless specified. The substrate temperature is attained using radiant heater.

4.7 Reflectivity Simulation

To verify the experimental results and to precisely calibrate the thickness measurement during the optical thin film deposition, we have carried out the reflectivity simulation of multilayer dielectric thin film coatings using LabVIEW (version 7.1). The reflectivity simulator is an essential tool in designing AR-HR coatings for facet-coating of laser diodes.

Figure 4.7 [a] and [b] show the front panel and block diagram of the LabVIEW program for reflectivity simulation. The details about the LabVIEW software will be discussed in the next chapter.

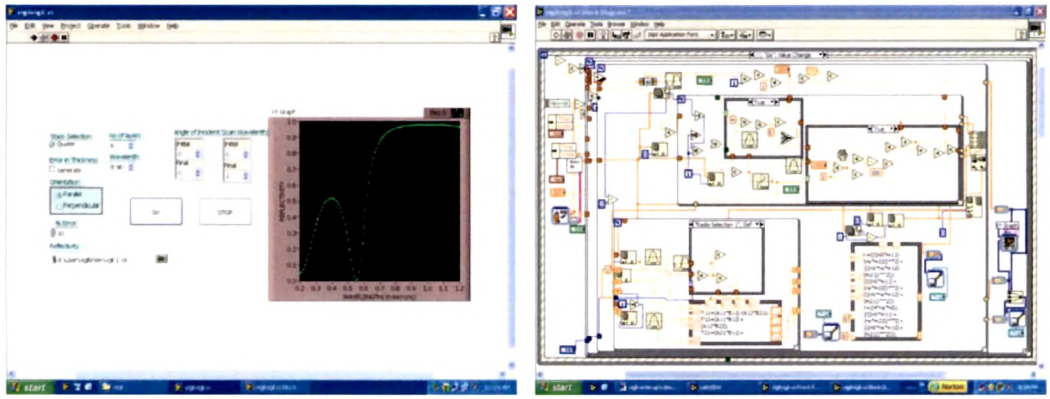

[a] [b]

Figure 4.7: Reflectivity simulation program [a] front panel and [b] block diagram.

The program simulates the reflectivity spectrum for the given range of wavelengths. For the calculation of reflection and transmission coefficients, the required input parameters like the wavelength range, wavelength step, number of layers and their refractive indices or file path of dispersion data, number of ensembles, and the angle step, are provided on the front panel of the virtual instrument. The program computes characteristic matrices for each individual layer of the multilayer stack of thin films at particular wavelength and from the product of these 2 X 2 matrices, a characteristic matrix of entire system is calculated. The reflectivity of the multilayer stack at given wavelength is then obtained using the equation,

$$R = \frac{(n_0 m_{11} - n_s m_{22})(n_0 m_{11} - n_s m_{22}) + (n_0 n_s m_{12} - m_{21})(n_0 n_s m_{12} - m_{21})}{(n_0 m_{11} + n_s m_{22})(n_0 m_{11} + n_s m_{22}) + (n_0 n_s m_{12} + m_{21})(n_0 n_s m_{12} + m_{21})}$$

The reflectivity of single layer or multilayer stack of thin films is calculated for a whole range of wavelength of interest and the simulated spectrum is displayed and stored for given set of data. The mathematical treatments [42] for derivation of above equation to calculate the reflectivity are given in appendix A.

4.8 Optical Thin Film Characterizations

Since, we are applying thin film optical coating for the reflectivity modulation, the main characterization necessary for our films is the reflectivity measurement. The AR and HR coatings are to be deposited on the facets of laser diode which are made up of GaAs based materials. However, it is not convenient to measure the reflectivity directly on the facet. So, we use GaAs substrate for measurement of the reflectivity. The GaAs substrate is kept in close vicinity of the laser diode bars during the deposition and thus we can assume that the thickness of various layers on the GaAs substrate is same as that on the laser diode facets. Initially we used the ex-situ reflectivity measurement setup for the optimization of AR-HR coatings. However, to get better precision and to save time and coating runs, we have also established in-situ reflectivity measurement during the later part of this work. These characterization setup and results are also discussed here.

4.8.1 Ex-situ Reflectivity Measurements

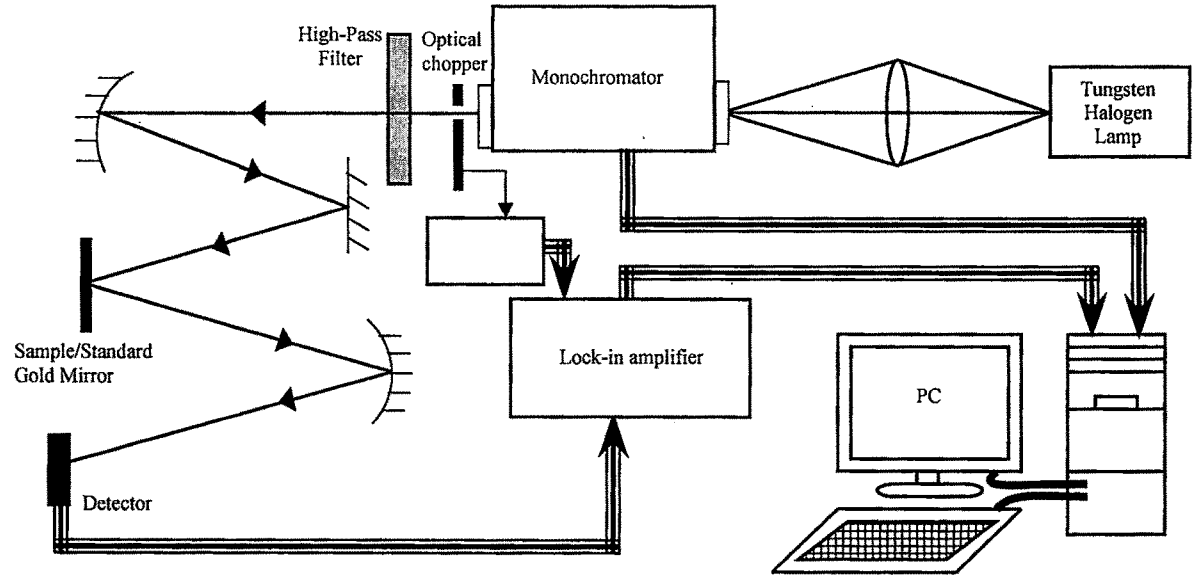

Figure 4.8: Block diagram of ex-situ reflectivity measurement setup.

Figure 4.8 shows the ex-situ reflectivity measurement setup established at our laboratory. Here, a Tungsten-Halogen lamp is used as a polychromatic light source. The light from the lamp is focused on the monochromator input slit using a convex lens. We have used

1/8m monochromator (CVI-CM110). The output beam from the monochromator is chopped using a mechanical chopper. The higher order wavelengths coming out of the monochromator are removed using an optical high-pass filter as shown in the figure 4.8. This chopped beam is then incident on the sample near-normal geometry and the reflected beam is directed to the photo-detector. The detector measures the intensity of the reflected beam with the help of lock-in amplifier (SR-530) and the reflectivity of the sample is measured in reference to the known values of reflectivity of a standard reflector, which is a gold coated mirror in our case. The actual photograph of the experimental setup is shown in figure 4.9.

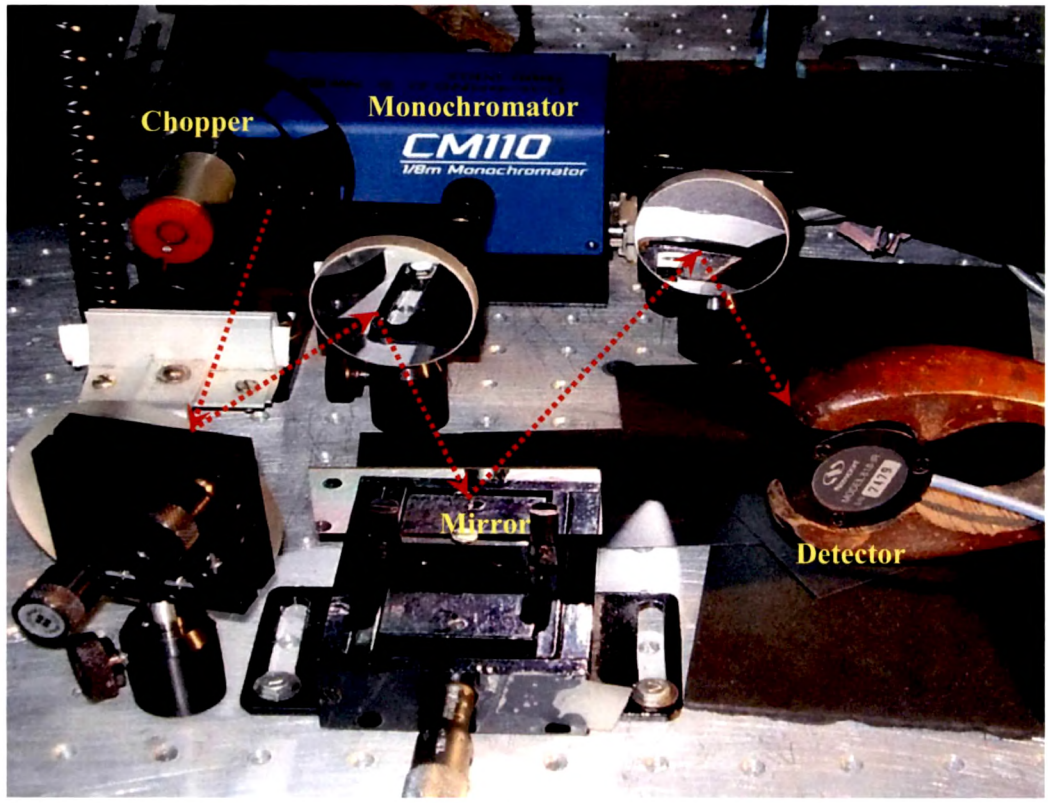

Figure 4.9: Photograph of ex-situ reflectivity measurement setup.

The reflectivity of the sample at particular wavelength is found using the equation,

$$R_S = \frac{S_S}{S_{GM}} R_{GM} \tag{4.9}$$

where, R_S is reflectivity of the sample, S_S is signal from the sample, S_{GM} is signal from the gold-mirror, and R_{GM} is the known reflectivity of the gold-mirror.

The monochromator and the lock-in amplifier have been interfaced with the computer using COM port and GPIB, respectively. The experiment is automated using LabVIEW. However in this setup, since the reflectivity of the sample is measured with reference to the standard reflectivity of gold-mirror, we need to take two scans for complete spectral range of interest; one with standard gold-mirror and the other with the unknown sample. This is a time consuming process. Moreover, the result is erroneous if the intensity of the source changes during the scan or between two scan due to input power fluctuation or some other reason. To avoid these problems, and to make the experiment fast and more accurate, we modified the setup with a beam-splitter. Figure 4.10 shows the modified experimental setup for ex-situ reflectivity measurement.

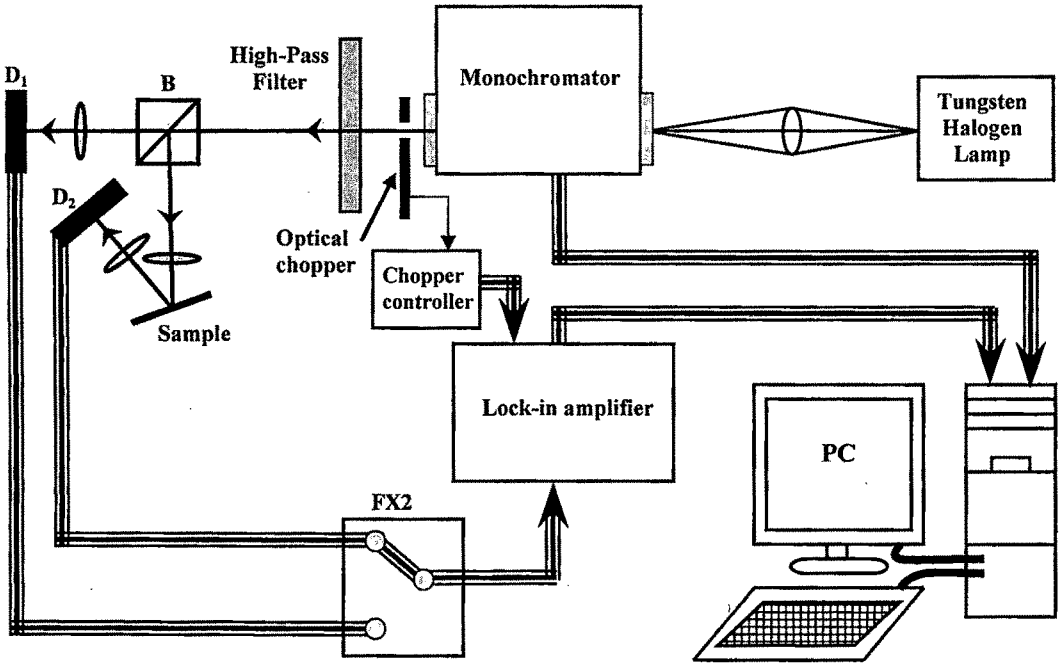

Figure 4.10: Block diagram of upgraded experimental setup for ex-situ reflectivity measurement.

In the modified setup, the output beam of the monochromator is split in to two beams by means of a cube beam-splitter B as shown in figure 4.10. Intensity of one beam is taken as a reference and measured directly with detector D_1 while the other beam is reflected from the test sample and measured by another detector D_2. The signals from these two detectors are fed to the lock-in amplifier through a programmable relay switch FX2. The reflectivity of the sample is the ratio of signals from two detectors with a constant multiplier, Y. The actual photograph of modified experimental setup is shown in figure 4.11.

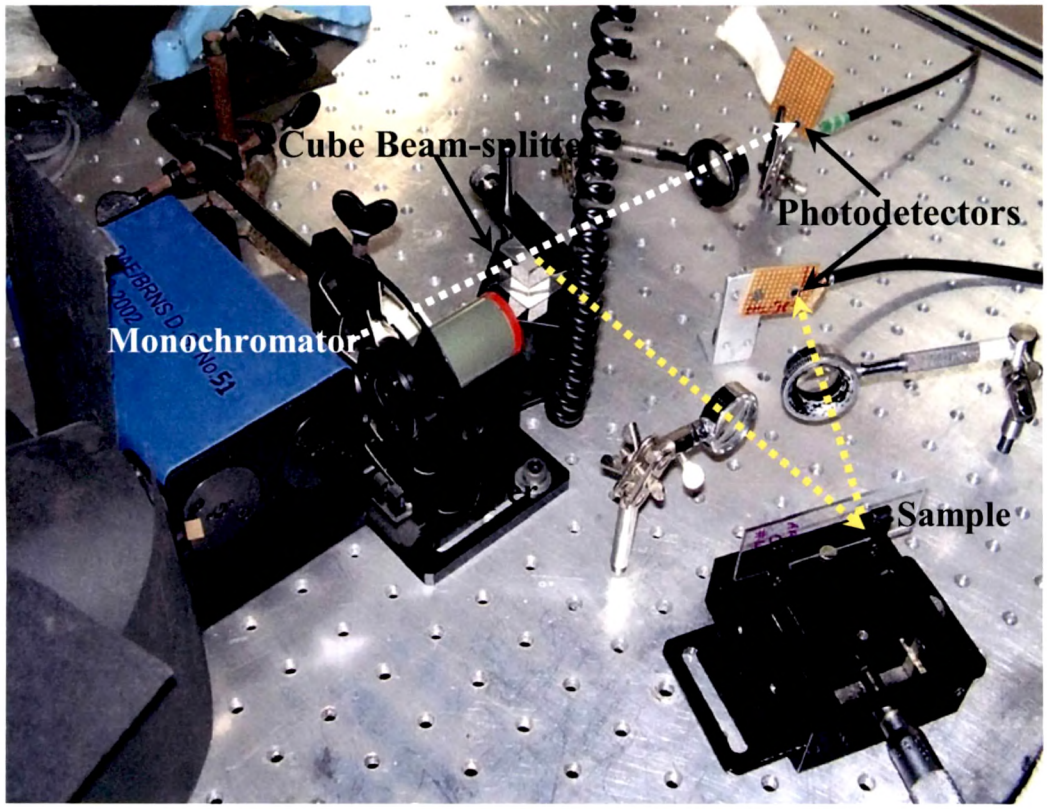

Figure 4.11: Photograph of upgraded ex-situ reflectivity measurement.

The dedicated virtual instrument, made in LabVIEW, computes and displays the reflectivity spectrum simultaneously with data acquisition and storage. Figure 4.12 [a] and [b] show the front panel (controls and displays) of the virtual instrument for reflectivity measurement displaying reflectivity spectrum of AR and HR coated test substrates.

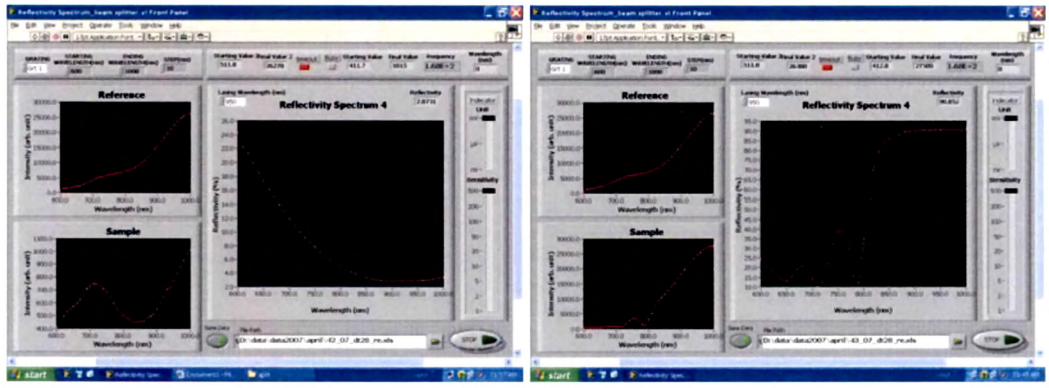

[a] **[b]**

Figure 4.12: Graphical user interface of VI for reflectivity measurement displaying results of [a] AR coated and [b] HR coated GaAs test substrates.

Figure 4.13 shows comparison of the reflectivity spectrum measured by earlier setup and the upgraded setup.

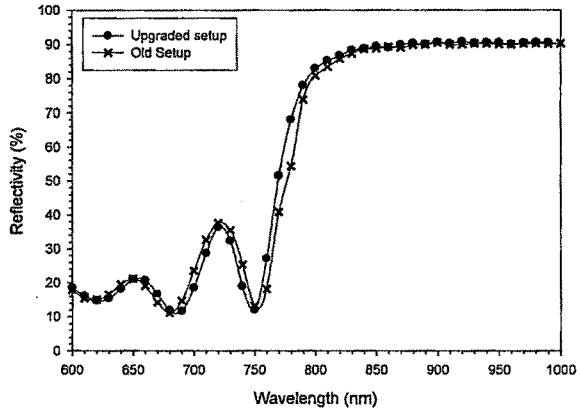

Figure 4.13: Reflectivity spectra measured in two different reflectivity measurement setups.

4.8.2 In-situ Reflectivity Measurements

Due to the nondestructive character and the real-time application, optical probe techniques such as reflectance-difference spectroscopy (RDS) [43,44], surface photo-absorption (SPA) [45], and Brewster angle reflectance spectroscopy (BARS) [46] have been developed and widely used for in-situ characterization of the growth of thin films. However, these techniques are complex and require very sophisticated instrumentations. We used the technique of measuring dynamic optical reflectance of the growing thin film for in-situ reflectivity measurement [47].

4.8.2.1 Experimental Setup

We have demonstrated a very simple, inexpensive and highly accurate in-situ reflectivity measurement setup using commonly available equipments. Initially we carried out the experiment with single layer only. We used MgF_2 as a low refractive index dielectric material. For optimization of the process, we deposited 5000 Å MgF_2 at two different deposition rate, i.e., 4 Å/sec and 10 Å/sec, as measured by quartz crystal monitor, on GaAs test substrates. The experiment was carried out at two different substrate temperatures i.e. at room-temperature and at 120 °C.

The experimental setup for in-situ reflectivity measurement is shown in figure 4.14. The laser diode used as a light source for the experiment is 657 nm red laser diode. BPW-34 photo detector is used to measure the intensity of reflected beam from the test substrate. The laser diode and the photo detector are arranged in the vacuum chamber as shown in figure 4.14. The laser diode is driven by ILX Lightwave LDP-3840 precision pulsed laser diode driver with 0.25% duty cycle and 400 ns pulse width through out the deposition run. SR530 Lock-in amplifier, synchronized with the current driver, acquires the signal from photo detector. The current driver and the Lock-in amplifier have been interfaced with PC using GPIB.

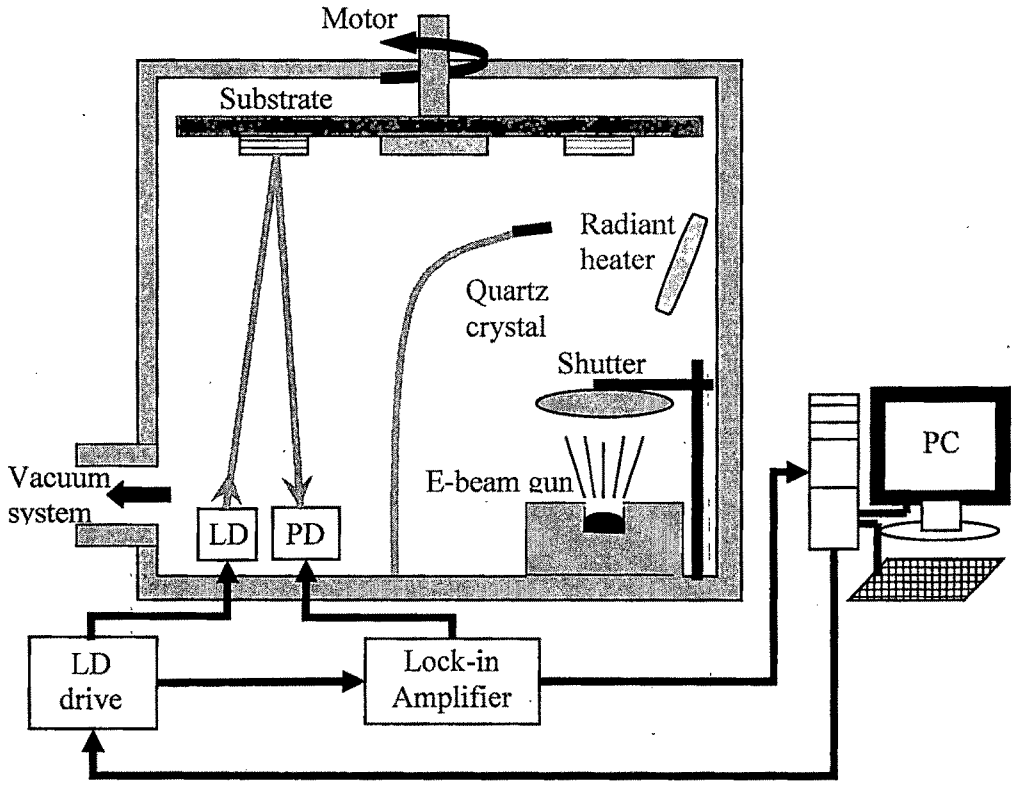

Figure 4.14: Block diagram of in-situ reflectivity measurement setup.

We have prepared a LabVIEW program, called Virtual Instrument (VI), to automate the whole experiment with total control over input current, duty cycle and pulse width of current, gain and sensitivity of Lock-in, delay time between two readings, and data storage. Figure 4.15 [a] shows the front panel controls and displays of the virtual instrument. The corresponding programming code, called block diagram, is shown in figure 4.15 [b].

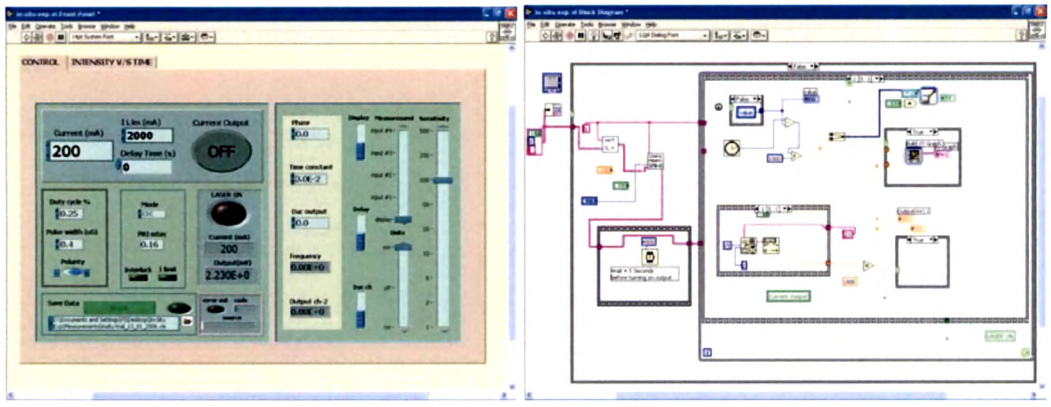

[a] [b]

Figure 4.15: [a] Front panel and [b] block diagram of the virtual instrument for in-situ reflectivity measurement.

4.8.2.2 Results and Discussion

Figure 4.16 shows the experimental and simulated reflectivity plots as function of MgF_2 film thickness deposited with the rate of 4 Å/sec. The film thickness is obtained dynamically by multiplying the constant deposition rate to the elapsed time.

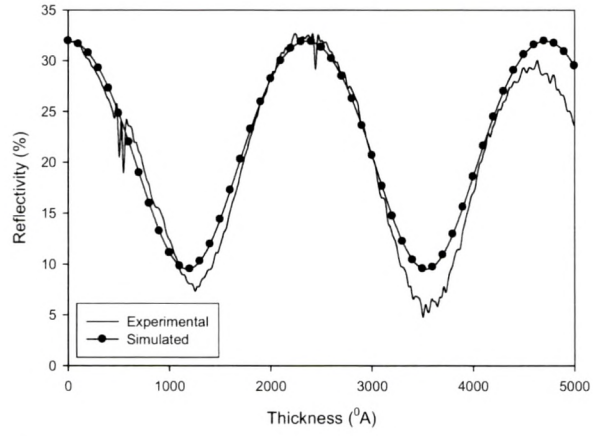

Figure 4.16: In-situ reflectivity plotted against depositing thickness, single layer MgF_2, rate 4 Å/sec, room-temperature.

As seen from figure 4.16, the experimental result is in good agreement with the simulated plot. However, the values of the valley points in the experimental plot decreases as the thickness increases, where as that in simulated plot remain constant. This deviation may be attributed to the assumption made in simulation that the refractive index

of the film remains constant throughout the deposition run. However, the refractive index of the film depends on the coating conditions like deposition rate and substrate temperature, and it changes slightly with the thickness. We also observed the deviation in the peaks from the simulated results after certain time. This is caused by the variation in the intensity of the source laser diode. At lower deposition rate, the process takes longer time and the laser diode intensity varies slightly due to high temperature. This problem does not occur in the case of higher deposition rate i.e. at 10 Å/sec. Figure 4.17 shows the reflectivity plot for the deposition run at 10 Å/sec.

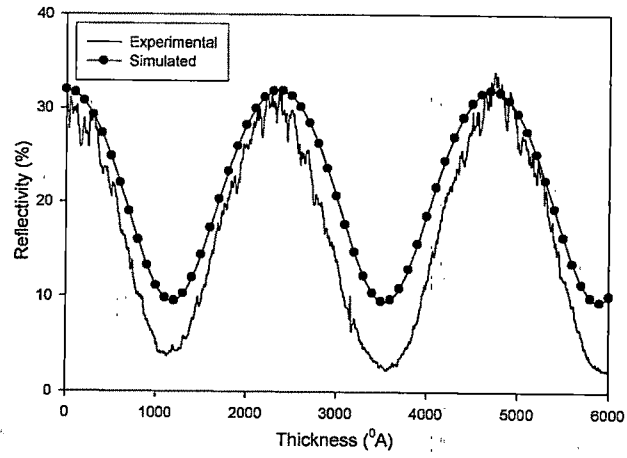

Figure 4.17: In-Situ reflectivity plotted against depositing thickness, single layer MgF_2, rate 10 Å/sec, room-temperature.

In this case, unlike the previous case, the upper peaks remain almost at constant level due to very less variation in the laser diode intensity because of smaller run time. However, with higher rate, the values of reflectivity, especially at the deeps deviates more from the theoretical plot due to change in the density and refractive index of the film at higher deposition rate. To minimize this deviation, we attempted the coating by increasing the substrate temperature. Figure 4.18 shows the reflectivity plot for the deposition at 120 °C substrate temperature with 10 Å/sec deposition rate. As seen from the figure 4.18, at higher temperature, the matching between the theoretical and experimental plots is better compare to that at room-temperature. We have not measured the refractive index of the film after deposition. The refractive index of bulk MgF_2 has been used for the calculation.

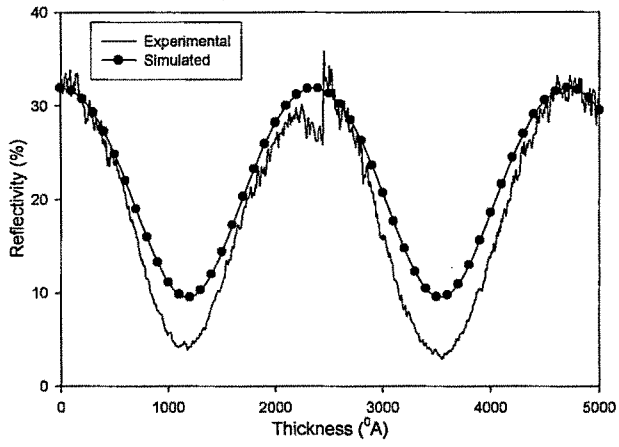

Figure 4.18: In-situ reflectivity plotted against depositing thickness, single layer MgF_2, rate 10 Å/sec, substrate temperature 120 °C.

The results are in good agreement with the theoretical plot at 10 Å/sec rate and 120 °C substrate temperature. However, the photo-detector signals are very noisy due to heating and glow generated during the deposition. Moreover, this setup was not efficient for multilayer coating, as in the case of HR coatings, where the deposition time is much longer than that of a single layer. This is because of rapid degradation of laser diode and photodetector inside the coating chamber due to high temperature. To overcome these limitations, we upgraded the in-situ reflectivity measurement setup.

4.8.2.3 Upgradation of In-situ Reflectivity Measurement

In the modified setup, we have taken laser diode and the detector outside the vacuum chamber. The beam is directed inside the chamber through a window with a special arrangement. With this modified setup, a significant improvement in signal to noise ratio is achieved.

The laser diode, as in the previous case, is driven by LDP-3840 precision pulsed current driver. However, In the modified setup, we used National Instrument's PCI-6024E Data Acquisition (DAQ) card, through BNC-2120 connector block to acquires the signal from photo detector instead of lock-in amplifier. The current driver has been interfaced with PC using GPIB. Figure 4.19 shows the block diagram of modified experimental setup and equipment interfacing for the experiment.

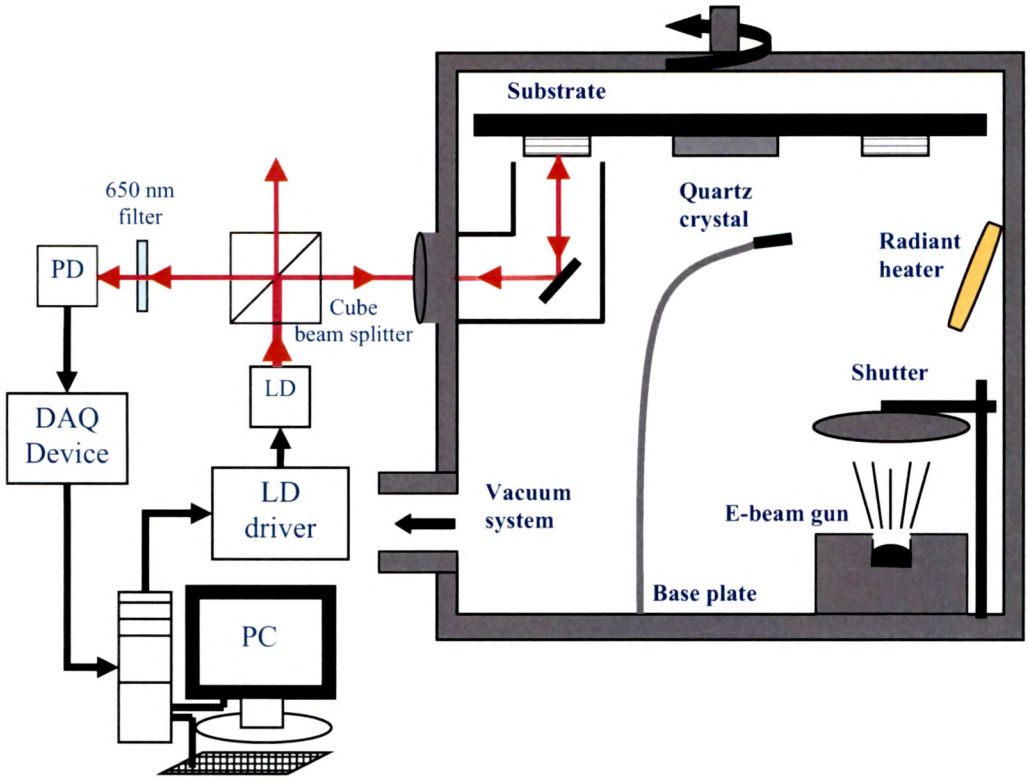

Figure 4.19: Block diagram of upgraded in-situ reflectivity measurement setup.

Figure 4.20 [a] and [b] show the front panel (controls and displays) and block diagram (programming codes) of the virtual instrument for modified setup.

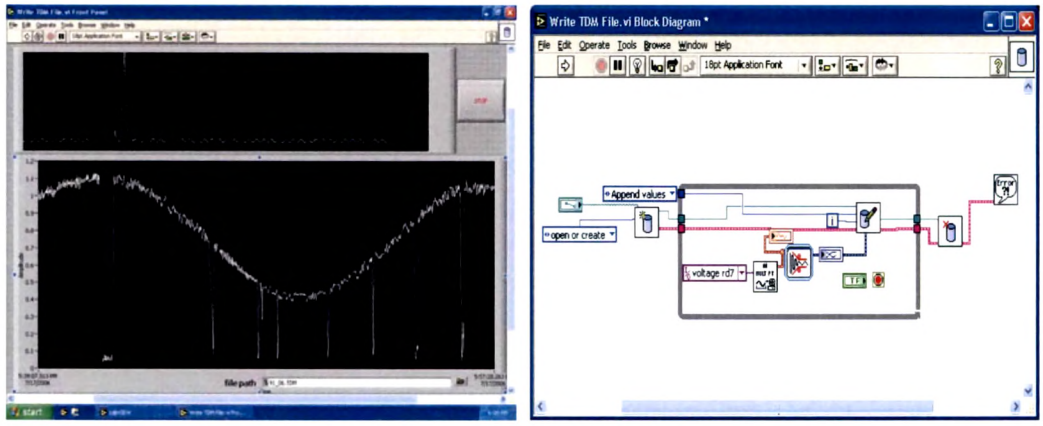

[a] **[b]**

Figure 4.20: [a] Front panel and [b] block diagram of virtual instrument for in-situ reflectivity measurement with beam-splitter.

Figure 4.21 shows the reflectivity measured in-situ during single layer MgF_2 deposition for AR coating on GaAs substrate. 5000 Å MgF_2 was deposited for the optimization of the system. The film thickness is obtained dynamically by multiplying the constant deposition rate to the elapsed time.

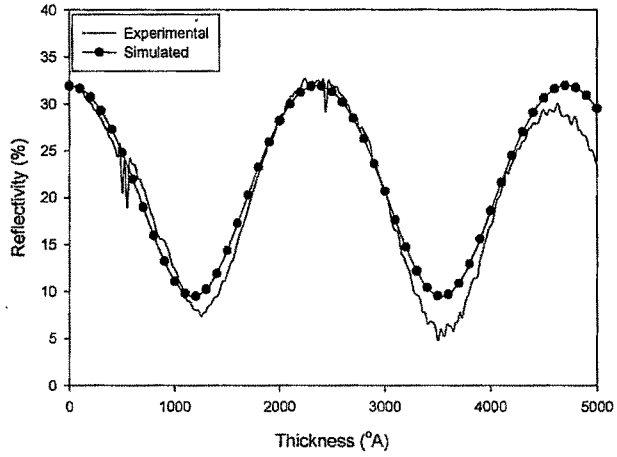

Figure 4.21: Reflectivity measured as a function of film thickness during deposition.

The reflectivity measurement during a pair of MgF_2-Si for HR coating is shown in Figure 4.22 [a]. The in-situ reflectivity is calculated with reference to the known reflectivity value of uncoated GaAs test substrate which is 32%. The results were confirmed by reflectivity spectrum of coated test substrates measured ex-situ after deposition as shown in Figure 4.22 [b].

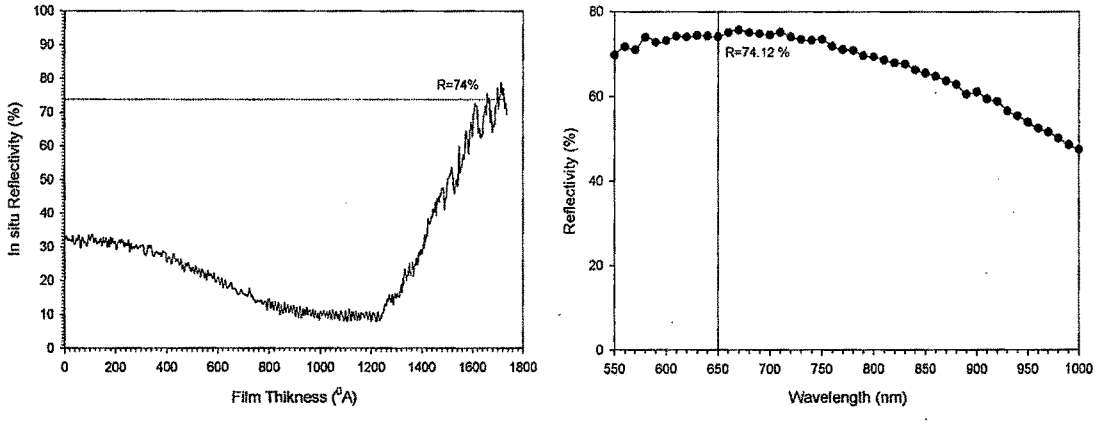

[a] [b]

Figure 4.22: [a] Insitu reflectivity as a function of film thickness during deposition, [b] reflectivity spectrum measured ex-situ; t_{MgF2}=1250 Å, t_{Si}=478 Å.

We also experimented with Al_2O_3 as a low refractive index material which could not be used for in-situ measurements in our earlier setup. However, in the modified setup,

we were able to improve the signal to noise ratio in data acquisition from the detector and successfully used Al_2O_3 that gives better reflectivity compare to MgF_2.

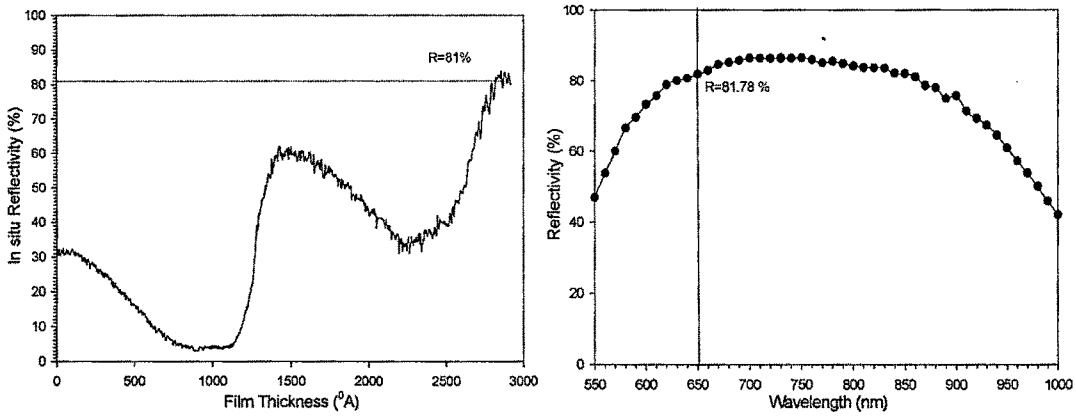

[a] [b]

Figure 4.23: [a] In-situ reflectivity as a function of thickness, [b] reflectivity spectrum measured after deposition t_{Al2O3}=979 Å, t_{Si}=478 Å.

Figure 4.23 [a] and figure 24 [a] show the in-situ reflectivity measured for two and three pairs of Al_2O_3-Si bi-layers respectively. The results were confirmed by ex-situ measurements as shown in figure 4.23 [b] and figure 24 [b].

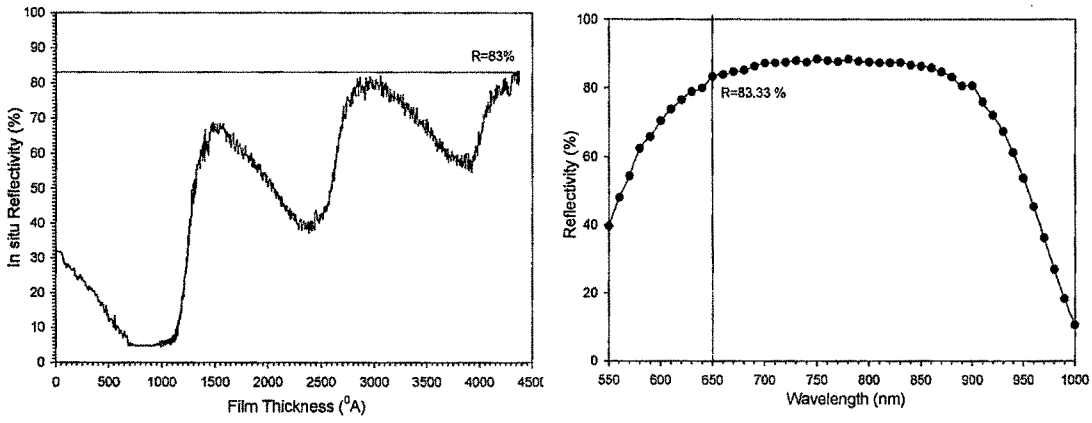

[a] [b]

Figure 4.24: Sample no. 109_06, Three pair Al2O3-Si, t_{Al2O3}=979 Å, t_{Si}=478 Å [a] in-situ reflectivity as a function of thickness, [b] reflectivity spectrum measured after deposition.

As seen from the figures, the results are in good agreement with the values of ex-situ. These results show that in-situ reflectivity measurements can be a very useful tool for the precise monitoring and control of optical thin films and can also be valuable for the complete automation of coating process.

4.9 Optimization of AR-HR Coatings for Different Wavelengths

We have designed AR and HR coatings for various laser diode structures with different lasing wavelength. These include 650 nm (Red), 820 nm, 850 nm, 890 nm, 950 nm, and 1200 nm laser diodes. The single layer and multilayer structures have been designed and optimized for respectively the AR film and the HR film on GaAs test substrates. The results of reflectivity measurement were compared with the simulated results. Finally, the optimize AR-HR coatings were applied to the facets of laser diode lasing at corresponding wavelength. The laser diodes were characterized before and after the facet-coatings in order to study the effects of facet-coatings. The L-I characteristics were measured on selected devices before and after AR-HR facet-coating in pulse-mode. The automatic characterization facility for laser diodes is setup in our laboratory and is described in detail in the next chapter.

4.9.1 650 nm

We used Al_2O_3 and Si as, respectively, low and high refractive index materials for AR-HR coatings of laser diode, lasing at 650 nm wavelength. The AR coating consists of single layer Al_2O_3. The HR coating is 3-pairs of Al_2O_3-Si bi-layers. The films of Al_2O_3 and Si were deposited at 200 °C substrate temperature and 120 rpm substrate rotation speed. The QWOT at 650 nm is 162.5 nm. Hence, the physical thickness of Al_2O_3 is 97.9 nm and that of Si to be 47.8 nm. Figure 4.25 [a] and [b] show the optimized reflectivity spectra for AR and HR coated GaAs test substrate respectively.

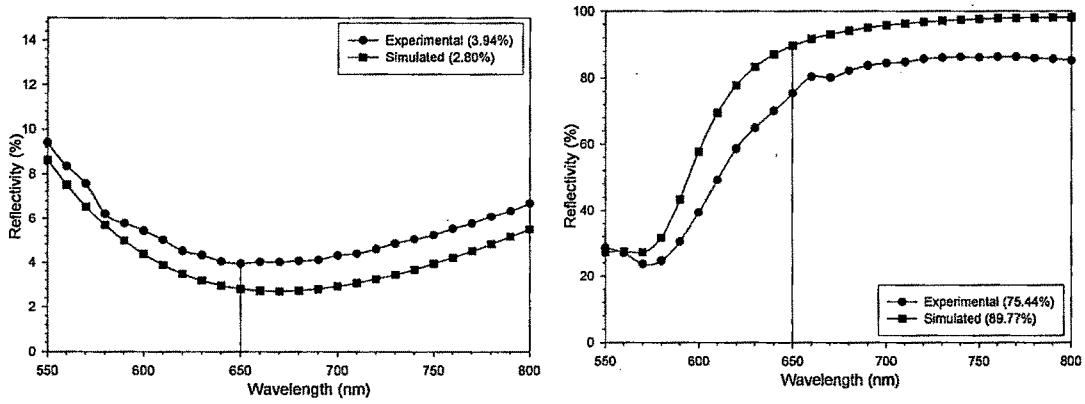

[a] [b]

Figure 4.25: Optimized simulated and experimental reflectivity spectra for [a] AR and [b] HR coated test substrate at 650 nm.

The reflectivity achieved with three pairs of bi-layers HR coating is low and there is a noticeable mismatch with simulated value. This may be attributed to the higher absorption of Si in this spectral range. Thus, for this wavelength and wavelength in visible range below 650 nm, Si should be replaced with suitable high refractive index materials. ZrO_2, Gd_2O_3 and other rare-earth oxides could be good alternative. However, the refractive indices of these materials are much low compared to silicon and require more number of bi-layers pairs.

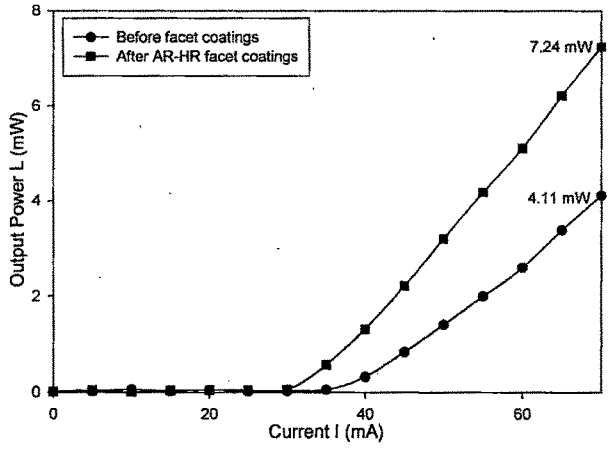

Figure 4.26: L-I Characteristics of 650 nm laser diode before and after facet-coating; $R_F = 3.94\%$, $R_R = 75.44\%$.

The effect of AR-HR facet-coating on L-I characteristic is shown in figure 4.26. The laser diodes used for the experiment are InGaAlP QW ridge waveguide laser diodes. The optical power from the AR coated facet is significantly enhanced from 4.11 mW to 7.24 mW at 70 mA.

4.9.2 820 nm

For 820 nm, we used single $\lambda/4$ thick Al_2O_3 film for the AR coating and stack of four pairs of $\lambda/4$ thick Al_2O_3 / $\lambda/4$ thick Si bi-layers for the HR coating. Figure 4.27 [a] and [b] show the optimized reflectivity spectra of AR and HR coated GaAs test substrates respectively for 820 nm. The QWOT at 820 nm is 205 nm, which gives the physical thickness for Al_2O_3 to be 123.4 nm and that for Si to be 60.2 nm.

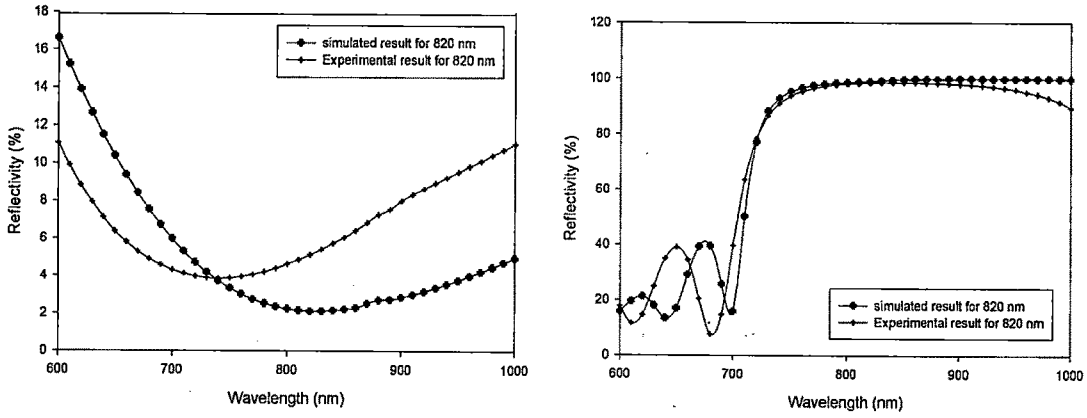

Figure 4.27: Optimized simulated and experimental reflectivity spectra for [a] AR and [b] HR coated test substrate at 820 nm.

The devices used are broad-area stripe lasers, operating at wavelength 820 nm. They have been fabricated from separately confined heterostructure of AlGaAs/GaAs/AlGaAs grown by liquid phase epitaxy [48,49]. The LPE grown laser devices used in the present work have about 3 % Al in the active region, which shifts the lasing wavelength to ~ 820 nm. The stripes used in this work are 100 - 200 μm wide. The length of the stripes ranges between 0.5 to 1.0 mm.

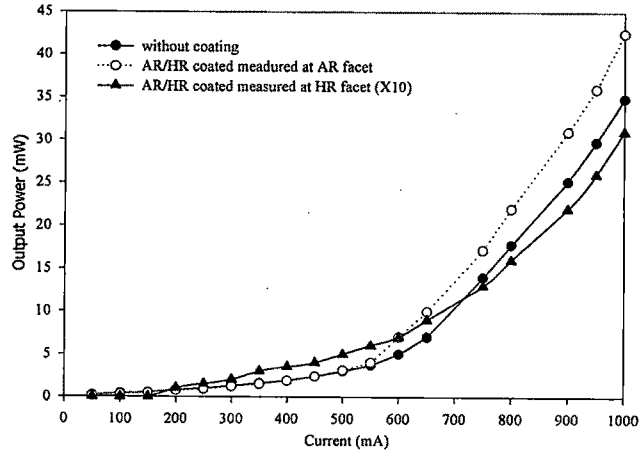

Figure 4.28: L-I Characteristics of 820 nm laser diode before and after facet-coating; $R_F = 5.08$ %, $R_B = 98.20$ %.

Figure 4.28 shows L-I characteristics of a device before and after deposition with AR-HR coatings. The L-I characteristics measurement were carried out using laser diode characterization facility at TIFR, Mumbai. The characteristics have been measured using

5 μs wide current pulses with duty cycle of 1%. Light is measured using an integrated sphere and a calibrated silicon detector. We see considerable reduction of light output from the HR coated facet. The reduction is consistent (almost by a factor of 10) as expected from the HR coated facet. Threshold current remains nearly the same after the coatings as prior to the coatings. Some enhancement of the power output is also seen from the AR coated facet. As such, the observed enhancement (~22%) at I ~ 1000 mA considerably less than expected (~90%). The exact reason for this behavior is not clear to us at present. The I–V characteristics of the devices measured after the coatings were not as good as obtained from the other typical uncoated devices. It is possible that there is some degradation of the device characteristics or mechanical damage to the device during the deposition of AR-HR coatings.

4.9.3 850 nm

We have used three bi-layer pairs for HR coating on 850 nm laser diodes. The actual structure is Substrate-LHLH...-Air. The same material combination, i.e., Al_2O_3 as a low refractive index layer (L) and Silicon as a high refractive index layer (H) was employed. For 850 nm, the quarter wave optical thickness is 212.5 nm for each layer. Therefore, the physical thickness for Al_2O_3 layer (L) is 128.0 nm and that for Si layer (H) is 62.5 nm. Figure 4.29 [a] and [b] show the experimental and simulated reflectivity spectra of AR and HR coated test substrate respectively optimized at 850 nm.

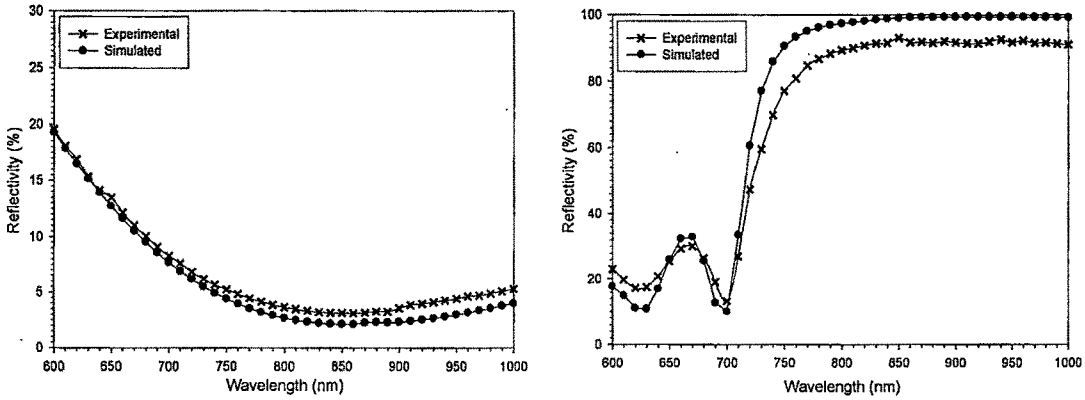

Figure 4.29: Optimized simulated and experimental reflectivity spectra for [a] AR and [b] HR coated test substrate at 850 nm.

The effect of AR-HR coating on L-I characteristics is shown in figure 4.30. The laser diode devices used for the experiment are GaAs QW laser diodes grown at Semiconductor Laser Section, Solid State Laser Division, RRCAT, Indore. In this case, the L-I characteristics were measured before and after coating using the laser diode characterization facility at RRCAT, Indore. As can be seen from the figure 4.30, the optical power from the AR coated facet enhances by almost 85% as expected after AR-HR facet-coatings.

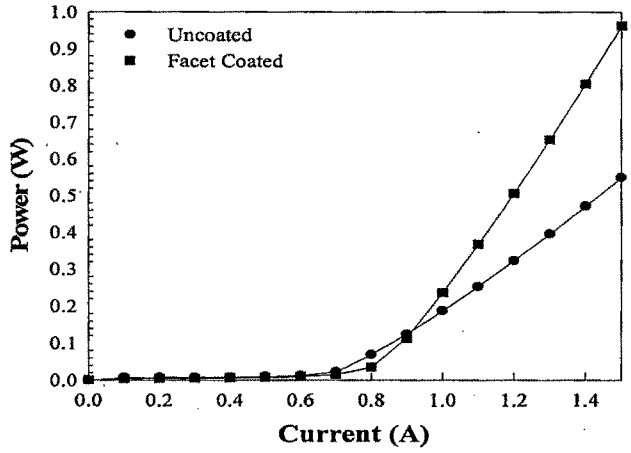

Figure 4.30: L-I characteristics of 850 nm laser diode before and after facet-coating; $R_F = 3.11$ %, $R_B = 91.54$ %

4.9.4 890 nm

We optimized AR-HR coating for 890 nm again using Al_2O_3 as low refractive index layers (L) and Silicon as a high refractive index layer (H).

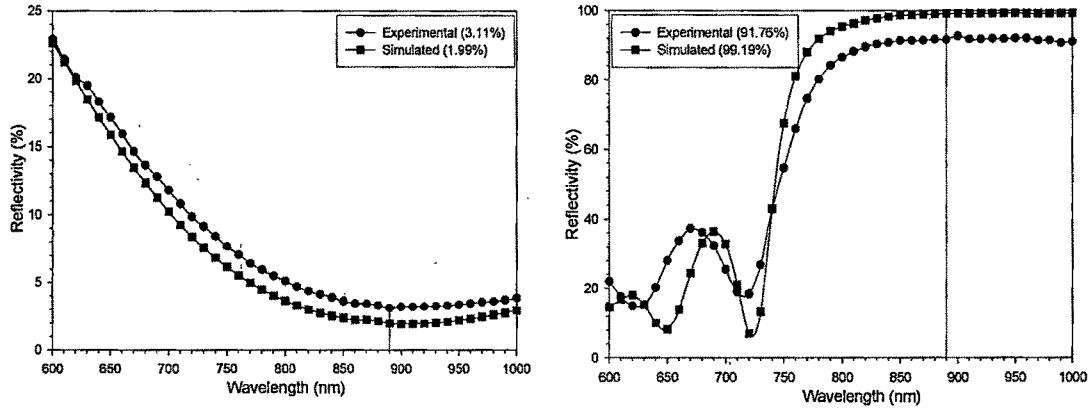

[a] [b]

Figure 4.31: Optimized simulated and experimental reflectivity spectra for [a] AR and [b] HR coated test substrate at 890 nm.

The HR coating is three bi-layer pairs of Al_2O_3-Si. For 890 nm, the quarter wave optical thickness is 222.5 nm for each layer. So, the physical thickness for Al_2O_3 (L) is 134.0 nm and that for Si layer (H) is 65.4 nm. Figure 4.31 [a] and [b] show the simulated and experimental spectra of respectively AR and HR coated test substrate.

The devices used for this experiment are The AlGaAs/GaAs/AlGaAs Double-Heterostructure (DH) laser diodes operating at 890 nm The effect of AR-HR facet-coating is shown in figure 4.32. The L-I characteristics measurements were carried out at our laboratory with automated laser diode characterization facility [50]. Here also, almost 86% enhancement is achieved in the optical power emission from the AR coated facet of the laser diode.

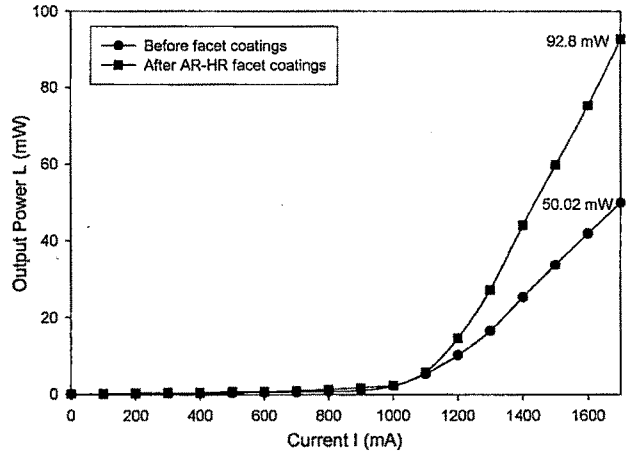

Figure 4.32: L-I Characteristics of 890 nm laser diode before and after facet-coating; $R_F = 3.98$ %, $R_B = 95.53$ %.

4.9.5 950 nm

We have used single layer Al_2O_3 for AR coating and four pairs of bi-layers Al_2O_3-Si for HR coating on laser diodes lasing at 950 nm. The actual structure of HR Coating is Substrate-LHLHLHLH-Air. In case of 950 nm, quarter wave optical thickness is 237.5 nm, giving the physical thickness of Al_2O_3 to be 143.0 nm and that of Si to be 69.8 nm. Figure 4.33 [a] and [b] show the simulated and experimental spectra of AR and HR coated test substrate respectively.

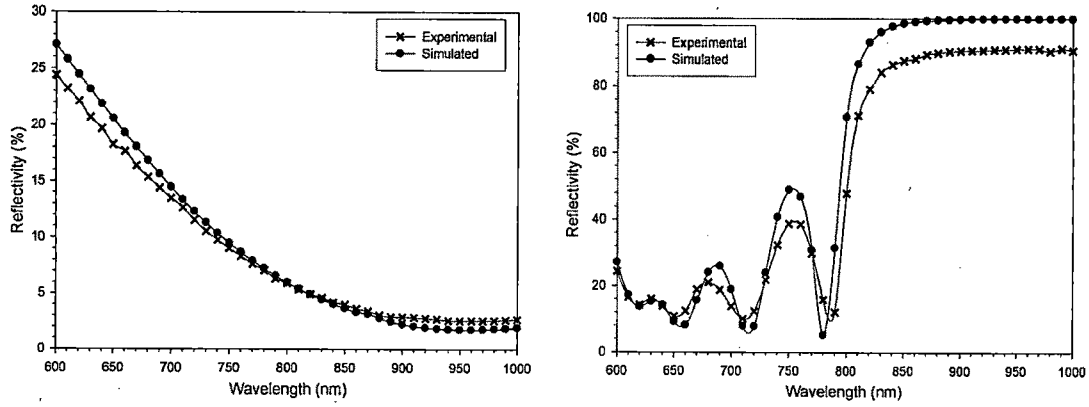

[a] [b]

Figure 4.33: Optimized simulated and experimental reflectivity spectra for [a] AR and [b] HR coated test substrate at 950 nm.

4.9.6 1200 nm

The optical thickness of AR coating film is one quarter of the lasing wavelength (λ/4) of laser diode. We used Al_2O_3 for single layer AR coating. We get as low as 2.78% reflectivity at 1200 nm from AR coated test substrate. The configuration for HR coating is a multi-layer stack of alternating films of high (H) and low (L) refractive index layers with (λ/4) optical thicknesses at the lasing wavelength. The actual structure of multi-layer stack for HR coating is Substrate-LHLHLH-Air. In this case too, Silicon has been used as a high refractive index layer (H) in our experiments. For designing HR coating for 1200 nm laser diode, the quarter wavelength (λ/4) optical thickness for each layer is 300 nm. So, the physical thickness for Al_2O_3 layer (L) is 187.5 nm and that for Silicon is 88.2 nm.

Figure 4.34 [a] and [b] show the experimental and the simulated reflectivity spectra of AR and HR coated test substrates respectively. As seen from figure 4.34 [b], the measured reflectivity of HR coated GaAs test substrate turns out to be 91.07 % at 1200 nm. The measured value is lower by around 8% as compared to the simulated value of the reflectivity at 1200nm in this case and in case of almost all the wavelengths discussed previously. This is mainly due to the usage of bulk values of the material parameters during reflectivity simulations. However, it is known that oxides film grown using e-beam evaporation exhibit a variation in refractive index with film thickness [51]. It is understood that the grown oxide film consists of a columnar structures which have a

large base diameter near the substrate and it keeps on decreasing with film thickness. This introduces porosity in the film varying along film thickness, leading to the refractive index inhomogeneity. Moreover, the materials used for dielectric coating are of a moderate purity (Al_2O_3:99.9%, Si: 98.5%). Hence, we anticipate some impurities in the grown layers which would further affect the measured value of reflectivity for HR stack.

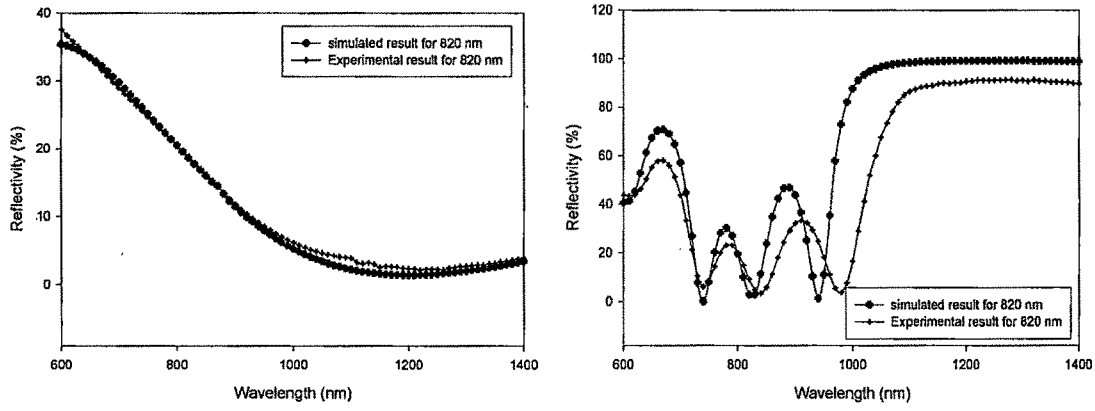

Figure 4.34: Optimized simulated and experimental reflectivity spectra for [a] AR and [b] HR coated test substrate at 1200 nm.

Highly strained InGaAs QW edge-emitting broad-area (BA) laser diodes used for these experiments are grown by MOVPE [52]. We have also carried out the analytical simulation of L-I characteristics for this particular diode structure using LabVIEW 7.1 [53]. The laser structure used for the experiment and the simulation consists of nominal 100-nm p^+ GaAs (cap layer)/1.55-μm p-$Al_{0.25}Ga_{0.75}As$ (upper cladding layer)/100-nm GaAs (waveguide layer)/8-nm InGaAs QW (active layer)/100-nm GaAs (waveguide layer)/ 2.2-μm n-$Al_{0.25}Ga_{0.75}As$ (lower cladding layer)/300-nm GaAs (buffer layer)/n^+ GaAs substrate.

In general, laser diode provides equal optical power from both, the front and the back facets. However, in most instances, only the power output from one of the facet is useful. So the optical power output from the front facet of laser diode is given by,

$$P_{OUT} = \frac{P_G}{2}\frac{(1-R_F)(1+R_B)}{(1-R_F R_B)} \tag{4.10}$$

Here, R_F and R_B are the reflectivity of the front and back facet of laser diode respectively. The total optical power generated in the cavity P_G is calculated as a function of input current I, as [54],

$$P_G = \eta_i \frac{\hbar\omega}{q}\left[\frac{\alpha_m}{\alpha_i + \alpha_m}\right](I - I_{th}) \tag{4.11}$$

Where, η_i and α_i are internal efficiency and internal loss respectively and are found from the plot of inverse differential efficiency versus cavity length shown in figure 4.35.

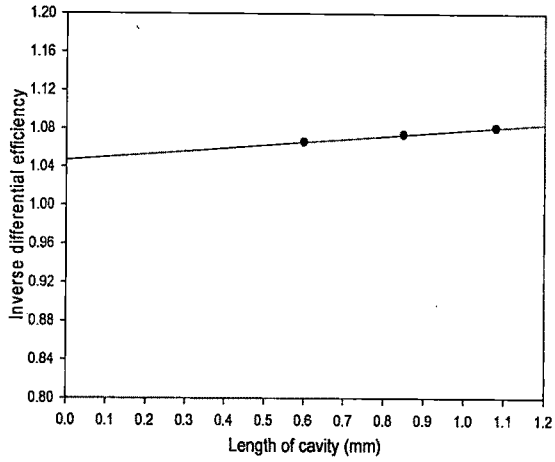

Figure 4.35: Inverse differential efficiency as function of cavity length.

The inverse differential efficiency is given as [55],

$$\frac{1}{\eta_D} = \frac{1}{\eta_i} + \frac{2\alpha_i}{n_i \ln\left(\frac{1}{R_F R_B}\right)} L \tag{4.12}$$

Therefore from the slope and intercept of the plot shown in figure 4.35, we get internal efficiency η_i to be 95.44% and the internal loss α_I is found to be 0.33 cm^{-1}.

In equation (4.11), α_m is mirror loss which is given as,

$$\alpha_m = \frac{1}{2L} \ln\left(\frac{1}{R_F R_B}\right) \tag{4.13}$$

I_{th} is the threshold current which is calculated from the definition of threshold current density, i.e.,

$$I_{th} = J_{th} LW \tag{4.14}$$

The threshold current density (J_{th}) for lower current range is obtained from gain current relation, where the gain is a logarithmic function of current density, as [56],

$$J_{th} = \frac{J_0}{\eta_i} \exp\left(\frac{\alpha_i + \alpha_m}{\Gamma \beta J_0}\right) \tag{4.15}$$

Here, β is the gain coefficient, Γ is optical confinement factor and J_0 is the transparency current density which is given by [57],

$$J_0 = eL_z B n_{tr}^2 \tag{4.16}$$

Here, L_z is quantum well width which is 80 Å in our case and n_{tr} is transparency carrier density. In equation (4.16), B is the bimolecular recombination co-efficient, and is given as,

$$B = \frac{e^2 L_z}{\epsilon_0 \, m_0^2 c^3 kT} \cdot \frac{n_{ra} E_g \left\langle M_{av}^2 \right\rangle}{(m_c + m_v)} \tag{4.17}$$

where, n_{ra} is the refractive index of active layer material and $\langle M^2_{av} \rangle$ is squared average momentum matrix element.

The transverse optical confinement factor, Γ, in equation (4.15) can be found by [58],

$$\Gamma = 4\pi^2 n_{ra} \Delta n_{ra} \left(\frac{d}{\lambda}\right)^2 \tag{4.18}$$

Here, d is the thickness of the active layer. Taking d = 8 nm for our structure, n_{ra}=3.67 for InGaAs active layer, and Δn_{ra}=0.331, we get the optical confinement Γ=0.00213. In equation (4.17), E_g is the energy band gap of active layer and is calculated for Strained $In_xGa_{(1-x)}As$ layer using [59]

$$E_g = 1.424 - 1.06x + 0.08x^2 \tag{4.19}$$

For 41% Indium content in the active layer, the energy band gap comes out to be 1.0028 eV. Taking m_c=0.048m_0 and m_v=0.365m_0 as found for strained $In_xGa_{1-x}As$ with

x=0.41 from the interpolation of their values for InAs and GaAs [60], and taking $<M^2_{av}>/m_0$ to be 8.70 eV [59], we get B=4.94 x 10^{-10} cm^3/s. Using this and taking transparency carrier density $n_{tr}=1.062\times10^{18}$ / cm^3, we get transparency current density $J_0=71.41$ A/cm^2.

The light output versus current (L-I) measurements were made on selected devices before as well as after the deposition of AR and HR coatings on the front and the back facets respectively. Measurements were carried out in pulsed-mode with 400 ns pulse-width and 0.25% duty-cycle. Figure 4.36 shows the L-I characteristics of laser diode before and after the coatings. The simulated L-I characteristics are also shown in figure 4.36.

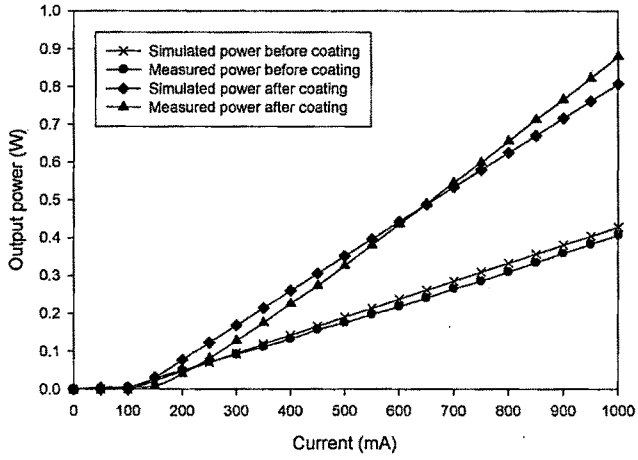

Figure 4.36: Simulated and measured L-I characteristics before and after facet-coatings; R_F = 2.78 %, R_B = 91.07 %, L=1.08mm, W=100 μm.

Significant enhancement of optical power output from the front facet of the laser diode due to AR-HR coatings on the facets can evidently be seen in figure 4.36. The application of HR coating on the back facet blocks the light emission from the rear facet and improves the effective efficiency of laser diode. It also lowers the lasing threshold current. The AR coating further increase the output power from front facet as well as protects the facet from COMD. Thus, the cumulative effect of AR and HR coating leads to boost the optical power output from front facet by almost 95% as seen in the figure 4.36. However, reduction in the front facet reflectivity leads to increase the mirror loss of cavity and subsequently increases the threshold current of laser diode. This effect is also clearly observed in the experimental result. The facet-coating also affects the external

differential quantum efficiency of laser diode. Increase of mirror loss as a result of change in the facet reflectivities causes the external differential efficiency to increase.

4.10 Conclusion

In conclusion, we have optimized AR-HR facet-coating for various wavelengths using single and multilayer dielectric thin films and applied these coatings on laser diodes lasing at different wavelengths. The in-situ reflectivity measurement setup has been established for characterization of optical thin films and is proved a very valuable technique for facet-coating of laser diodes. The effects of facet-coatings on laser diode characteristics have been studied for a large number of laser diode structures. The facet-coating improves the effective efficiency of laser diode and protects the laser diode facet from environmental effects and other degradation. Thus, facet-coating with appropriate dielectric materials is a vital step in the fabrication of high-power laser diodes.

➢ References

[1] O. Ueda, "*Reliability and Degradation of III-V Optical Devices*", Artech House, London, (1996)

[2] C.H.Henry, P.M.Petroff, R.A.Logan, F.R.Merritt, *J. Appl. Phy.*, **50(5)**, pp. 3721, (1979)

[3] H.H.Lee, L. Figueroa, *J. Electrochem. Soc.*, **135**, pp. 496, (1988)

[4] C.D.Thurmond, G.P.Schwartz, G.W.Kammlott, B.Schwartz, *J. Electrochem. Soc.*, **127**, pp. 1366, (1980)

[5] W. C. Tang, H. J. Rosen, P. Vettiger, D. J. Webb, *Appl. Phys. Lett.*, **59**, pp. 1005 (1991)

[6] P.W. Epperlein, *Proc. SPIE*, **3001**, In-Plane Semiconductor Lasers: from Ultraviolet to Midinfrared; Ed.: Hong K. Choi, Peter S. Zory, pp. 13, (1997)

[7] J.M. Rommel, P. Gavrilovic, F.P. Dabkowski, *J. Appl. Phys.*, **80**, pp. 6547, (1996)

[8] U. Menzel, R. Puchert, A. Barwolff, A. Lau, *Microelectron. Reliability*, **38**, pp. 821, (1998)

[9] R. Schatz, C.G. Bethea, *J. Appl. Phys.*, **76**, pp. 2509, (1994)

[10] G. Zhang, A. Ovtchinnokov, J. Nappi, H. Asonen, M. Pessa, *IEEE J. Quant. Electron.*, **29**, pp. 1943, (1993)

[11] M. Ohkubo, S. Namiki, T. Ijichi, A. Iketani, T. Kikuta, *IEEE J. Quant. Electron.*, **29**, pp. 1932, (1993)

[12] D. Botez, "High power Al-free diode lasers", *Compound Semicond. Magazine*, **5**, pp. 24, (1999)

[13] Juan Jimenez, *C. R. Physique*, **4**, pp. 663, (2003)

[14] A. Valster, A. T. Meney, J. R. Downes, D. A. Faux, A. R. Adams, A. A. Brouwer, A. J. Corbijn, *IEEE J. Sel. Topics Quantum Electron.*, **3**, pp. 180, (1997)

[15] P. Collot, J. Arias, V. Mira, E. Vassilakis, F. Julien, *SPIE Proc.*, **3628**, pp. 260, (1999)

[16] M. Watanabe, K. Tani, K. Takahashi, K. Sasaki, H. Nakatsu, M. Hosoda, S. Matsui, O. Yamamoto, S. Yamamoto, *IEEE J. Sel. Topics Quantum Electron.*, **1**, pp. 728, (1995)

[17] L. W. Tu, E. F. Schubert, M. Hong, G. J. Zydzik Meyer, *J. Appl. Phys.*, **80**, pp. 6448, (1996)

[18] A. J. Howard, C. I. H. Ashby, J. A. Lott, R. P. Schneider, R. F. Corless, *J. Vac. Sci. Technol.*, **A 12**, pp. 1063, (1994)

[19] H. Imai, M. Morimoto, H. Sudo, T. Fujiwara, M. Takusagawa, *Appl. Phys. Lett.*, **33**, pp. 1011, (1978)

[20] H. Brugger, P. W. Epperlein, *Appl. Phys. Lett.*, **56(11)**, pp. 1049, (1990)

[21] J. A. Caballero, C. He, and S. Djavani-Tabrizi, T. Yin, R. Mallard, S. R. Das, *J. Vac. Sci. Technol.*, **A (22) 3**, pp. 865, (2004)

[22] R. D. Dupuis, R. L. Hartman, F. R. Nash, *IEEE Electron. Device Lett.*, **EDL-4(8)**, pp. 286, (1983)

[23] V. Kummler, A. Lell, and V. Harle, U. T. Schwarz, T. Schoedl, W. Wegscheider, *Appl. Phy. Lett.*, **84(16)**, pp. 2989, (2004)

[24] J. Sacher, W. Elsasser, E. O. Gobel, H. Jung, *Electronic Letters*, **27(16)**, pp. 1463, (1991)

[25] A. Mar, P. A. Morton, J. E. Bowers, *Electronic Letters*, **26(17)**, pp. 1382, (1990)

[26] T. Guhne, V. Gottschalch, G. Leibiger, H. Herrnberger, J. Kovac, J. Kovác, Jr., R. Schmidt-Grund, B. Rheinländer, D. Pudis, *Laser Physics*, **16(3)**, pp. 441, (2006)

[27] R. Wyatt, W. J. Devlin, *Electronic Letters*, **19**, pp. 110, (1983)

[28] G. Eisenstein, R. S. Tucker, U. Koren, S. K. Korotky, *IEEE J. Quant. Electron.*, **QE-22**, pp. 142, (1986)

[29] T. Saitoh, T. Mukai, *Electronic Letters*, **23**, pp. 218, (1987)

[30] R. C. Steele, I. W. Marshall, *Electronic Letters*, **23**, pp. 296, (1987)

[31] G. Eisentein, R. M. Jopson, *Int. J. Electron.*, **60**, pp. 113, (1986)

[32] G. C. Dente, M. L. Tilton, *IEEE J. Quantum Electron.*, **29**, pp. 76, (1993)

[33] Hirokazu Shimizu, Kunio Itoh, Takashi Sugino, Masaru Wada, Iwao Teramoto, *IEEE J. Quant. Electron.*, **QE-19(3)**, pp. 470, (1983)

[34] Y. Yamamoto, "Coherence, Amplification and Quantum Effects in Semiconductor Lasers", John Wiley & Sons, New York, (1990)

[35] H. A. Macleod, "*Thin Film Optical Filters*", 2nd Edn., pp. 25, Adam Hilger Ltd, Bristol, (1986)

[36] O. S. Heavens, "*Thin Film Physics*", pp. 78, Methuen & Co. Ltd, London, (1970)

[37] Eisenstein G., Stulz L. W., *Appl. Opt.*, **23**, pp. 161, (1984)

[38] M. Passlack, C. G. Bethea, W.S.Hobson, John Lopata, E.F. Schubert, G.J.Zydzik, D. T. Nichols, J.F. de Jong, U. K. Chakrabarti, N. K. Dutta, *IEEE J. Select. Topics Quant. Electron.*, **1(2)**, pp. 110, (1995)

[39] S. Guha, E. Cartier, N.A. Bozarczuk, J. Bruley, L. Gignac, J. Karasinski, *J. Appl. Phy.*, **90**, pp. 512, (2001)

[40] G. Eisenstein, L. W. Stulz, L. G. Van Uitert, *J. Lightwave Tech.*, **LT-4**, pp. 1373, (1986)

[41] A. Chambers, R. K. Fitch, B. S. Halliday, "Basic Vacuum Technology", 2nd Edn., pp. 10, CRC Press, (1998)

[42] Eugene Hecht, "*Optics*", 4th Edn., Pearson Education, (2004)

[43] D.E. Aspnes, W.E. Quinn, M.C. Tamargo, M.A.A. Pudensi, S.A. Schwarz, M.J.S.P. Brasil, R.E. Nahory, S. Gregory, *Appl. Phys. Lett.*, **60(10)**, pp. 1244, (1992)

[44] D.E. Aspnes, J.P. Harbison, A.A. Studna, L.T. Florez, *Appl. Phys. Lett.*, **52(12)**, pp. 957, (1988)

[45] N. Kobayashi, T. Makimoto, Y. Yamauchi, Y. Horikoshi, *J. Cryst. Growth*, **107(1-4)**, pp. 62, (1991)

[46] N. Dietz, H.J. Lewerenz, *Appl. Surf. Sci.*, **69**, pp. 350, (1993)

[47] Chetan Panchal, Vipul Kheraj, Pravin Patel, Krunal Pandya, Tarun Kumar Sharma, *Proc. SPIE*, **6286 (62860H)**, Advances in Thin-Film Coatings for Optical Applications III; Ed.: Michael J. Ellison (2006)

[48] S. S. Chandvankar, A. P. Shah, A. Bhattacharya, K. S. Chandrasekaran, B. M. Arora, *J. Cryst. Growth*, **260**, pp. 348, (2004)

[49] A. P. Shah, M. R. Gokhle, A. Bhattacharya, B. M. Arora, *Proc. Intl. Conf. on Fibre Optics and Photonics (Photonics-2000)*, **1**, pp. 206, (2000)

[50] V. A. Kheraj, P. K. Patel, C. J. Panchal, T. K. Sharma, *Proc. of Sixth DAE-BRNS National Laser Symposium (NLS-6)*, Indore, India, pp. 70, (2006)

[51] Samuel Pellicori, *Coating Materials News*, **13 (2)**, pp. 1, (2003)

[52] T. K. Sharma, M. Zorn, F. Bugge, R. Hulsewede, G. Erbert, M. Weyers, *IEEE Photon. Tech. Lett.*, **14(7)**, 887, (2002)

[53] V. A. Kheraj, C. J. Panchal, P. K. Patel, B. M. Arora, T. K. Sharma, *Journal of Optics and Laser Technology*, **39(7)**, pp. 1395, (2007)

[54] Peter Unger, "*Introduction to power diode lasers*", High Power Diode Lasers, Ed.: R. Diehl, *Topics Appl. Phys.*, **78**, pp. 31, Springer-Verlag Berlin Heidelberg, (2000)

[55] David G. Mehuys, "*High-Power Semiconductor Lasers*", Semiconductor Laser II: Material & Structure, Ed.: Eli Kapan, pp. 259, Academic Press; (1999)

[56] James J. Coleman, "*Strained Layer Quantum Well Heterostructure Lasers*" Quantum Well Lasers, Ed.: Peter S. Zori Jr., pp.367, Academic Press, Inc, (1993)

[57] A.Ghiti, M. Silver, E. P. O'Reilly, *J. Appl. Phys*, **71(09)**, pp. 4626, (1992)

[58] B. R. Nag, "*Physics of Quantum Well Devices*", Kluwer Academic Publishers, (2000)

[59] Scott W. Corzine, Ran-Hong Yan, Larry A. Coldren, "*Optical Gain in III-V Bulk and Quantum Well Semiconductors*", Quantum Well Lasers, Ed.: Peter S. Zori Jr., pp.17, Academic Press, Inc., (1993)

[60] D. J. Hall, T. J. C. Hosea, C. C. Button, "*Semicond. Sci. Technol.*", **13**, pp. 302, (1998)